Available online at www.sciencedirect.com
SCIENCE DIRECT®
Journal of the Mechanics and Physics of Solids
53 (2005) 2347–2383
JOURNAL OF THE MECHANICS AND PHYSICS OF SOLIDS
www.elsevier.com/locate/jmps

One-dimensional response of sandwich plates to underwater shock loading

V.S. Deshpande*, N.A. Fleck

Cambridge University, Engineering Department, Trumpington Street, Cambridge, CB2 1PZ, UK

Received 11 July 2004; received in revised form 28 June 2005; accepted 29 June 2005

Abstract

The one-dimensional shock response of sandwich plates is investigated for the case of identical face sheets separated by a compressible foam core. The dynamic response of the sandwich plates is analysed for front face impulsive loading, and the effect of strain hardening of the core material is determined. For realistic ratios of core mass to face sheet mass, it is found that the strain hardening capacity of the core has a negligible effect upon the average through-thickness compressive strain developed within the core. Consequently, it suffices to model the core as an ideally plastic-locking solid. The one-dimensional response of sandwich plates subjected to an underwater pressure pulse is investigated by both a lumped parameter model and a finite element (FE) model. Unlike the monolithic plate case, cavitation does not occur at the fluid–structure interface, and the sandwich plates remain loaded by fluid until the end of the core compression phase. The momentum transmitted to the sandwich plate increases with increasing core strength, suggesting that weak sandwich cores may enhance the underwater shock resistance of sandwich plates.

Keywords: Sandwich plates; Dynamic plasticity; Fluid–structure interaction; Lattice materials

*Corresponding author. Fax: +44 1223 332662
E-mail address: vsd@eng.cam.ac.uk (V.S. Deshpande).

0022-5096/$ - see front matter © 2005 Elsevier Ltd. All rights reserved.
doi:10.1016/j.jmps.2005.06.006

1. Introduction

It is well known that sandwich beams possess a superior bending stiffness and strength to monolithic beams of the same mass under quasi-static loading. Much less is known about the dynamic performance of sandwich beams subjected to air and underwater shocks; this is the topic of the current investigation.

Parallel studies by Fleck and Deshpande (2004) and Xue and Hutchinson (2004) have demonstrated that sandwich beams have superior shock resistance to monolithic beams. While Fleck and Deshpande (2004) developed an analytical model for the shock resistance of clamped sandwich beams, Xue and Hutchinson (2004) conducted 3D dynamic finite element (FE) simulations to investigate the response of clamped sandwich beams to impulsive loadings. In assuming impulsive loading, both studies decoupled the fluid–structure interaction phase from the structural response. This assumes that the time period for fluid–structure interaction is much shorter than the structural response time for plastic bending and stretching of the beam. However, in sandwich structures, core compression typically precedes the stretching and bending of the beam and it is unclear whether the fluid–structure interaction phase can be decoupled from the core compression phase.

Recently, Rabczuk et al. (2004) have investigated the response of sandwich beams subjected to underwater shocks by performing fully coupled FE fluid–structure interaction simulations while Mäkinen (1999) employed a one-dimensional finite difference scheme to investigate the fluid–structure interaction of polymer foam core sandwich beams with composite face sheets. These calculations suggest that the benefits of employing sandwich construction for shock mitigation applications might be overestimated by the analysis of Fleck and Deshpande (2004) and Xue and Hutchinson (2004). A questionable assumption is the decoupling of the fluid–structure interaction phase from the core compression phase. We examine in detail this interaction by performing a fairly complete one-dimensional study of the dynamic core compression of a sandwich plate by a shock wave, with the aim of establishing the regimes of validity of the analyses of Fleck and Deshpande (2004) and Xue and Hutchinson (2004).

The outline of the paper is as follows. First, the shock resistance of the sandwich core is investigated by assuming impulsive loading on the front face sheet. Finite element simulations of the one-dimensional fluid–structure interaction problem are reported, and the development of cavitation in the fluid is discussed. Motivated by the FE results, a lumped parameter model is developed for this interaction and is used to construct a fluid–structure interaction map showing the various possible regimes of behaviour. The FE and lumped parameter models are compared, and the effects of the magnitude of core strength, shock impulse and sandwich plate mass upon the level of transmitted impulse into the structure are investigated.

2. Impulse response of sandwich plates

Consider a sandwich plate comprising two identical rigid face sheets each of mass m_f, and a core of thickness c and mass m_c made from a rigid crushable plastic

material. In this section, we present the one-dimensional response of the sandwich plate for the case where impulsive-type shock loads are applied uniformly to the front face of the sandwich plates; that is, an initial velocity $v_0 = I_0/m_f$ is imparted to the face sheet, where I_0 is the shock impulse per unit area. The rationale for replacing the finite pressure-time pulse associated with the shock by an initial velocity imparted to the front face of the sandwich plate rests on the fact that the decay period of the incoming shock wave is much shorter than the structural response time of the sandwich plates. This assumption has been employed in previous studies (Fleck and Deshpande, 2004; Xue and Hutchinson, 2004) and its quality will be investigated in Section 3.

2.1. Models for core compression

It is assumed that the incoming shock wave imparts a velocity $v_0 = I_0/m_f$ to the front face sheet; the advancing front face sheet then crushes the core. During this crushing event the front face is decelerated by the core whilst the core and the rear face sheet are accelerated. The core is treated as a rigid, ideally plastic foam-like solid; it compresses at a constant strength σ_c with no lateral expansion up to a densification strain ε_D, beyond which it is rigid, see Fig. 1a. This type of constitutive law is not only representative of that for metal foams (Ashby et al., 2000) but also of that for other stacked, periodic cellular sandwich cores such as the prismatic-diamond and stacked pyramidal cores (Wadley et al., 2004). The rigid, perfectly plastic locking (rppl) solid has already been introduced by Reid and Peng (1997). It is properly interpreted as the limit the limit of an elastic-hardening solid, with the elastic modulus tending to infinity and the plastic modulus tending to zero. The neglect of elastic deformation of the core is justified for the case when the time for multiple elastic wave reflections in the core is much less than the time for plastic wave propagation through the core. This is expected to be true for most metallic cellular solids since the elastic wave speeds in these solids are much higher than the plastic

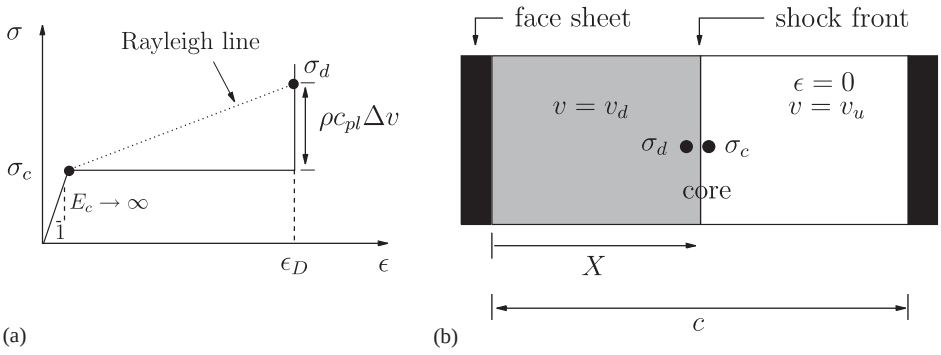

Fig. 1. (a) Idealised quasi-static stress versus strain response of the foam core with the Rayleigh line for the jump condition across a plastic shock in such a foam. (b) Sketch of the propagation of a one dimensional shock wave in a foam core of the sandwich plate.

wave speed. Similarly, the assumption of rigid face sheets is acceptable when the transit time for multiple elastic wave reflections in the face sheets is much less than the time for plastic wave propagation in the core. This is justified as the faces are much thinner than the core and are made from fully dense materials.

We proceed to present two candidate models for the dynamic response of the sandwich plate. Both models aim to predict the degree of core compression up to the point when the velocities of the two face sheets equalise.

2.1.1. Model A: assumption of quasi-static dissipation in core

Let v_f be the final common velocity of the core and two face sheets. Momentum conservation dictates that

$$v_f = \frac{I_0}{2m_f + m_c}. \tag{1}$$

Thus, the ratio of the energy lost U_{lost} in the core compression to the initial kinetic energy of the outer face sheet is given by

$$\frac{U_{\text{lost}}}{m_f v_0^2/2} = \frac{1+\bar{m}}{2+\bar{m}}, \tag{2}$$

where $\bar{m} \equiv m_c/m_f$. In model A, assume that all the lost energy U_{lost} is dissipated in compressing the core, and neglect rate effects within the core. Then, we have

$$U_{\text{lost}} = \sigma_c \varepsilon_c c, \tag{3}$$

where ε_c is the nominal core compression strain. Combining (2) and (3) gives

$$\varepsilon_c = \frac{\varepsilon_D}{2}\frac{1+\bar{m}}{2+\bar{m}}\hat{I}^2, \tag{4}$$

in terms of the dimensionless impulse $\hat{I} \equiv I_0/\sqrt{m_f c \sigma_c \varepsilon_D}$. It is deduced from (4) that ε_c reaches the densification strain ε_D when $\hat{I}$ attains the value $\sqrt{2}((2+\bar{m})/(1+\bar{m}))^{1/2}$. At larger values of $\hat{I}$, ε_c is set to the limiting value of ε_D and additional dissipation mechanisms must be involved for energy conservation. This analysis does not explicitly model any such mechanisms but it does assume their existence. We note in passing that rate independent finite element simulations make similar assumptions to model A.

The above treatment using global energy and momentum conservation analysis is unable to furnish additional details, such as the progression of core compression with time and the period T_c required for the face sheets and core to the attain the final common value v_f.

2.1.2. Model B: analysis of plastic shock wave propagation in the core

The above analysis is rigorous in giving the average through-thickness compression strain ε_c, assuming that the only dissipation mechanism is rate-independent plastic compression of the core. In reality, the core compresses non-uniformly due to inertial effects, and a plastic shock wave propagates through the core. The dissipated energy can far exceed the quasi-static result (3) with additional

dissipation mechanisms such as material rate sensitivity and heat conduction typically coming into play.

Consider the sandwich plate described above with face sheets each of mass m_f per unit area and a core of mass m_c per unit area and thickness c. The front face sheet has an initial velocity $v_0 = I_0/m_f$ while the core and rear face sheet are initially at rest. As assumed above, the core is a rigid-ideally plastic solid with strength σ_c and a nominal densification strain ε_D beyond which it is rigid. After impact of the front face sheet against the adjacent core and rear face, a plastic shock wave is initiated in the core and travels through the core at a Lagrangian speed $c_{\rm pl}$. Because of the rigid nature of the initial response, it is assumed that the stress immediately ahead of the shock front has been raised to σ_c by the "elastic precursor" wave. After time t the shock wave has advanced a distance X (measured in the undeformed configuration), as sketched in Fig. 1b. At this instant, the undeformed core upstream from the shock wave and the rear face sheet share a velocity v_u; downstream from the shock wave the core has been compressed to a strain ε_D and the compressed core and front face sheet share the velocity v_d. The average through-thickness strain in the core is $\varepsilon_c \equiv \varepsilon_D X/c$. Global conservation of momentum dictates that

$$m_f v_0 = \left[m_c \frac{X}{c} + m_f\right] v_d + \left[m_c\left(1 - \frac{X}{c}\right) + m_f\right] v_u, \tag{5}$$

while conservation of mass across the shock dictates that the plastic shock wave speed $c_{\rm pl}$ is

$$c_{\rm pl} = \dot{X} = \frac{v_d - v_u}{\varepsilon_D}. \tag{6}$$

Here, the over-dot indicates differentiation with respect to time. As mentioned above, the precursor wave has brought the foam to yield on the upstream side of the shock front. Consequently, the acceleration of the foam and rear face sheet is obtained by integrating the Lagrangian equilibrium relation

$$\frac{\partial \sigma}{\partial X} + \rho \ddot{u} = 0, \tag{7}$$

where ρ is the density of the material (in the undeformed configuration). Integrating (7) from the unsupported rear face sheet to the shock front gives

$$\sigma_c = \left[m_f + m_c\left(1 - \frac{X}{c}\right)\right] \dot{v}_u = \left[m_f + m_c\left(1 - \frac{X}{c}\right)\right] \frac{{\rm d}v_u}{{\rm d}X}\, c_{\rm pl}. \tag{8}$$

After substituting for $c_{\rm pl}$ from (6) and integrating from the initial condition $v_u = 0$ at $X = 0$, the above differential equation is solved to give

$$\hat{I}^2(\bar{m} + 2)\bar{v}_u^2 - 2\hat{I}^2 \bar{v}_u - \left[\bar{X} + \left(\frac{\bar{m} + 2}{\bar{m}}\right) \ln\left(1 - \frac{\bar{m}\bar{X}}{1 + \bar{m}}\right)\right] = 0, \tag{9}$$

where $\bar{v}_u \equiv v_u/v_0$ and $\bar{X} \equiv X/c$. With this choice of non-dimensional groups, the final common velocity of the face sheets and core is $\bar{v}_u = 1/(\bar{m} + 2)$, and (9) provides an implicit relation for the value $\bar{X}_f \equiv \varepsilon_c/\varepsilon_D$ at which the plastic shock wave arrests

within the core,

$$\frac{\hat{I}^2}{2(\bar{m}+2)}+\left[\bar{X}_f+\left(\frac{\bar{m}+2}{\bar{m}}\right)\ln\left(1-\frac{\bar{m}\bar{X}_f}{1+\bar{m}}\right)\right]=0. \tag{10}$$

We note in passing that at impulses exceeding the limit,

$$\hat{I}^2\geqslant\frac{2(\bar{m}+2)^2}{\bar{m}}\left[\ln(1+\bar{m})-\frac{\bar{m}}{2+\bar{m}}\right], \tag{11}$$

the core densifies completely and ε_c attains the densification strain ε_D.

We proceed to estimate the energy dissipation rate in propagating the plastic shock wave at a speed $c_{\rm pl}$. The form of the momentum balance across a singular surface is given by (Bland, 1988)

$$[\sigma]-\rho c_{\rm pl}[v]=0, \tag{12}$$

where [ ] denotes the jump of the respective quantities across the shock. Substituting for $c_{\rm pl}$ from (6) then gives the stress σ_d on the downstream side of the shock front as

$$\sigma_d=\sigma_c+\frac{(v_d-v_u)^2}{\varepsilon_D}=\left[m_f+m_c\frac{X}{c}\right]\dot{v}_d, \tag{13}$$

as shown by the Rayleigh line in Fig. 1a. By employing the expressions (8) and (13) for $\dot{v}_u$ and $\dot{v}_d$, respectively, the rate of energy dissipation $\dot{E}$ can be shown to be given by

$$\dot{E}=\frac{1}{2}(\sigma_c+\sigma_d)\varepsilon_D c_{\rm pl}=\sigma_c\varepsilon_D c_{\rm pl}+\frac{m_c}{2c}c_{\rm pl}^3\varepsilon_D^2, \tag{14}$$

Note that the term $\sigma_c\varepsilon_D c_{\rm pl}$ is the energy dissipation rate assuming that the maximum energy absorption capacity of the foam core per unit volume is $\sigma_c\varepsilon_D$ (area under the quasi-static stress versus strain curve up to full densification up to full densification). The ratio γ of the dynamic energy dissipation rate $\dot{E}$ to the maximum quasi-static energy dissipation rate $\sigma_c\varepsilon_D c_{\rm pl}$ is

$$\gamma=1+\frac{m_c}{2c\sigma_c}c_{\rm pl}^2\varepsilon_D\geqslant 1, \tag{15}$$

implying that a dissipative mechanism must exist in addition to the quasi-static plastic dissipation mechanism. A detailed description of dissipation within the shock requires additional constitutive assumptions. For example, the assumption that the core strength is rate dependent leads to a shock of finite thickness, but with the jump conditions across the shock remaining unchanged, see for example Radford et al. (2005). Additional dissipative mechanisms involving a characteristic length or time (e.g. heat conduction, texture) can also provide structure for the shock wave. However, for the present purpose of determining the compressive strain profile through the core, details of the shock structure are not required and the present analysis suffices.

As discussed in Duvall (1973), a solid with a Hugonoit of the form sketched in Fig. 1a is expected to form two shocks. The dynamic foam compression analysis

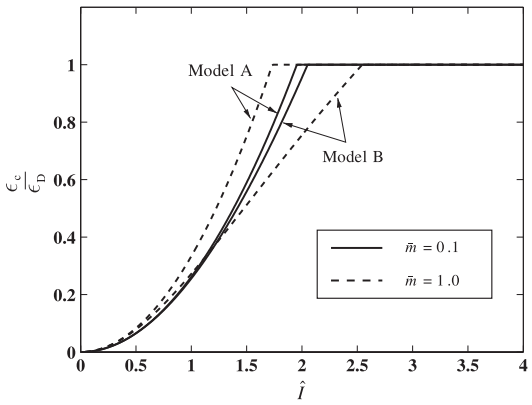

Fig. 2. Core compression as a function of the normalised shock impulse for two choices of the core to face sheet mass ratio $\bar{m}$. Results are shown for models employing the quasi-static energy dissipation (Model A) and the plastic shock wave propagation model (Model B).

presented here is essentially a two-wave solution: one Rayleigh line for the elastic precursor (with elastic modulus $E_c \to \infty$) takes the unstressed foam to yield while the second Rayleigh line for the plastic shock is given by (13) and sketched in Fig. 1a. Thus, this model is analogous to the rigid–plastic-locking models for the dynamic compression of foams presented by Ashby et al. (2000) and Tan et al. (2002).

The prediction (10) of the core average compression strain $\varepsilon_c \equiv \bar{X}_f \varepsilon_D$ is plotted against the applied impulse $\hat{I}$ in Fig. 2 for $\bar{m}$ equal to 0.1 and 1.0. The figure includes the prediction (4) of Model A (quasi-static energy dissipation in core). Model A predicts that for any given value of $\hat{I}$, ε_c is larger for $\bar{m} = 1.0$ than for $\bar{m} = 0.1$. This is consistent with the fact that the level of kinetic energy absorbed by plastic dissipation within the core increases with increasing $\bar{m}$. On the other hand, the shock wave propagation model (marked as model B in Fig. 2) predicts that for any given value of $\hat{I}$, ε_c is larger for $\bar{m} = 0.1$ than for $\bar{m} = 1.0$; this is consistent with the fact that the energy ratio γ as defined by (15) increases with increasing core mass m_c. Further, the shock propagation model always predicts a smaller compression of the core than the quasi-static, energy dissipation model. Note that a realistic value of $\hat{I}$ is approximately 1.5 for an intense water-borne shock, based upon the choice $I_0 = 10^4\,\mathrm{Ns\,m^{-2}}$, $m_f = 80\,\mathrm{kg\,m^{-2}}$, $c = 100\,\mathrm{mm}$, $\varepsilon_D = 0.5$ and $\sigma_c = 10\,\mathrm{MPa}$.

Experiments on the dynamic compression of metallic foams confirm that the compression of the foam is non-uniform due to the propagation of a plastic shock wave, see for example Radford et al. (2005). Further, in Appendix A we show that the core compression predictions of the shock wave propagation model are in excellent agreement with full finite element simulations.[1] Thus, the shock wave

[1]This confirms the accuracy of the rppl model for the core and provides justification for the neglect of elastic wave effects in the core and face sheets.

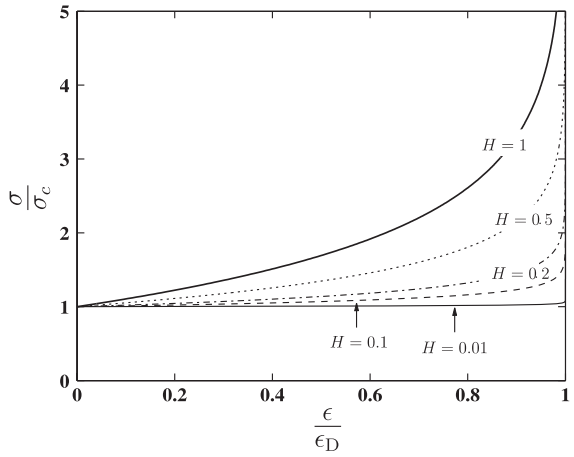

Fig. 3. The compressive nominal stress versus strain response (16) of a sandwich core for selected values of the hardening parameter H.

model B developed above is expected to capture the dynamic core compression more accurately than the quasi-static energy dissipation model A and we employ the shock wave model in all subsequent analysis.

2.2. *Effect of strain hardening*

In the above shock wave analysis, the quasi-static stress versus strain response is assumed to be ideally plastic up to the densification strain ε_D. In reality, most cellular core materials, such as the prismatic diamond core strain harden. We proceed to extend the shock wave core compression model to account for strain hardening within the core. Specifically, we assume that the core is a rigid, plastic material with stress σ versus plastic strain ε response described by

$$\frac{\varepsilon}{\varepsilon_D} = 1 - \exp\left[\frac{1}{H}\left(1 - \frac{\sigma}{\sigma_c}\right)\right], \tag{16}$$

where σ_c is the yield strength of the core and H is a non-dimensional hardening parameter. Eq. (16) is sketched in Fig. 3 for five choices of the hardening parameter H. The figure clearly indicates that the strain hardening rate decreases with decreasing H, and the ideally plastic response is recovered in the limit $H \to 0$. For all practical purposes, (16) has reduced to the ideally plastic case at $H = 0.01$.

A plastic shock wave analysis is now presented for the sandwich plate with a strain hardening core. Consider again the sandwich plate as described in Section 2.1.2. At time t, the shock has travelled a distance X into the core, and the velocities of the regions upstream and downstream from the shock are v_u and v_d, respectively. The elastic precursor has brought the material to incipient yield immediately upstream of the shock front. Thus, momentum and mass conservation across the

shock dictate that

$$\sigma_d = \sigma_c + \frac{m_c c_{\rm pl}(v_d - v_u)}{c} \tag{17a}$$

and

$$c_{\rm pl} = \frac{v_d - v_u}{\bar{\varepsilon}}, \tag{17b}$$

respectively, where σ_d is the stress on the downstream side of the shock front, associated with the strain $\bar{\varepsilon}$. Now substitute the stress σ_d from (17) into the constitutive law (16) to obtain an implicit relation for the strain jump $\bar{\varepsilon}$

$$H\hat{I}^2\left[\frac{1-\bar{v}_d(2+\bar{m})}{(1+\bar{m}\bar{X})}\right]^2 + \frac{\bar{\varepsilon}}{\varepsilon_D}\ln\left(1-\frac{\bar{\varepsilon}}{\varepsilon_D}\right) = 0, \tag{18}$$

and substitute $c_{\rm pl}$ from (17) into (8) to obtain the governing differential equation for the motion as

$$\frac{{\rm d}\bar{v}_u}{{\rm d}\bar{X}} = \frac{1}{\hat{I}^2[1+\bar{v}_u(2+\bar{m})]}\,\frac{(1+\bar{m}\bar{X})}{1+\bar{m}(1-\bar{X})}\,\frac{\bar{\varepsilon}}{\varepsilon_D}. \tag{19}$$

The solution of (19), with initial condition $\bar{v}_u = 0$ at $\bar{X} = 0$, provides the dependence of the velocities $\bar{v}_u$ and $\bar{v}_d$ upon $\bar{X}$. For a sufficiently low value of the initial velocity v_0 (or equivalently impulse $\hat{I}$), the shock wave arrests in the core at $\bar{X} = \bar{X}_f$ when $\bar{v}_u = \bar{v}_d = 1/(2+\bar{m})$; the final nominal compressive strain of the core, and the corresponding time T_f at which the shock wave arrests in the core, are given by

$$\frac{\varepsilon_c}{\varepsilon_D} = \int_0^{\bar{X}_f}\frac{\bar{\varepsilon}}{\varepsilon_D}\,{\rm d}\bar{X}, \tag{20}$$

and

$$\frac{T_f v_0}{c\varepsilon_D} = \int_0^{\bar{X}_f}\frac{\bar{\varepsilon}}{\varepsilon_D(\bar{v}_d - \bar{v}_u)}\,{\rm d}\bar{X}, \tag{21}$$

respectively. However, for large values of $\hat{I}$, the shock wave travels through the entire core before the velocities $\bar{v}_u$ and $\bar{v}_d$ have attained their final values $1/(2+\bar{m})$. In such cases we assume that the velocities become equalised immediately after the shock wave has reached the rear face sheet, and ε_c and T_f are given by (20) and (21), respectively, upon taking $\bar{X}_f = 1$.

The predictions of the above analysis are shown in Figs. 4–6 for two choices of the mass ratio, $\bar{m} = 0.1$ and 1.0. The variation of ε_c with $\hat{I}$ is shown in Fig. 4a and b for $\bar{m} = 0.1$ and 1.0, respectively. For the case $\bar{m} = 0.1$, an increase in the core hardening rate H leads to a decrease in ε_c; in contrast, for the choice $\bar{m} = 1.0$, the core strain ε_c is nearly insensitive to the value of H. These trends are a consequence of the fact that the dynamic energy dissipation rate is much greater than the quasi-static dissipation rates for high density cores, see Eq. (15). The position $\bar{X}_f$ at which the shock arrests is plotted in Figs. 5a and b for the $\bar{m} = 0.1$ and 1.0 cases, respectively. At any given value of $\hat{I}$, increased hardening diffuses the strain profile within the core and causes

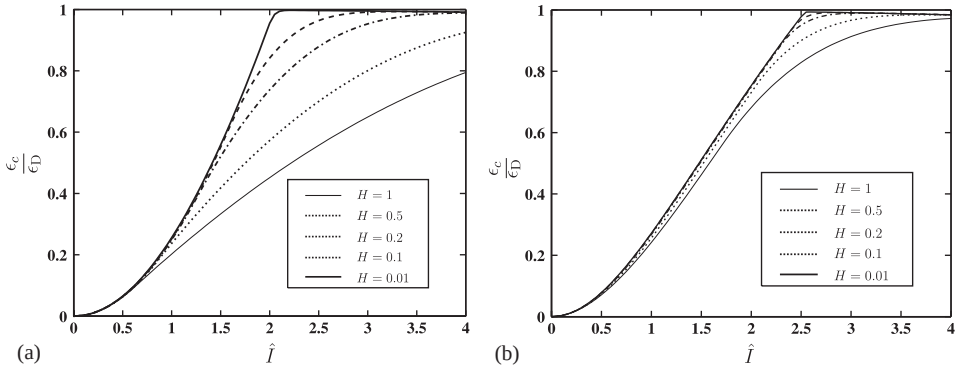

Fig. 4. Core compression as a function of the shock impulse for selected values of the core hardening rate H. Results are shown for core to face sheet mass ratios (a) $\bar{m} = 0.1$ and (b) $\bar{m} = 1.0$.

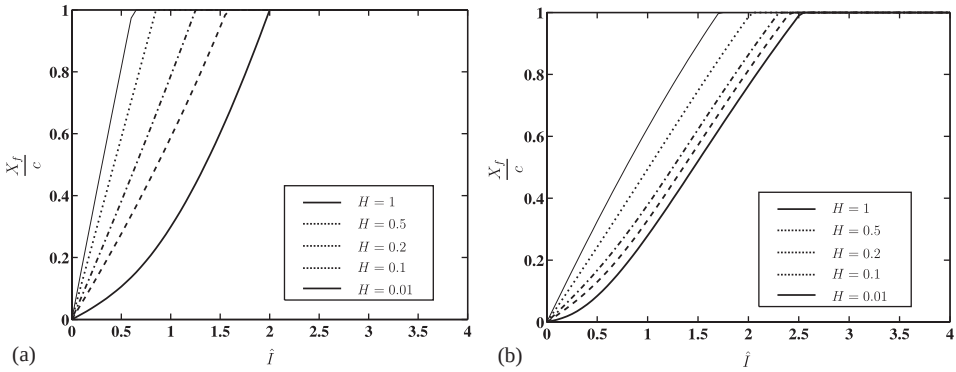

Fig. 5. Normalised shock front arrest position as a function of the shock impulse for selected values of the core hardening rate H. Results are shown for core to face sheet mass ratios (a) $\bar{m} = 0.1$ and (b) $\bar{m} = 1.0$.

the shock wave to travel further into the core (larger value of $\bar{X}_f$). The speed of the shock wave also increases with increasing hardening, and consequently the core compression time T_f decreases with increasing H, see Fig. 6.

The above investigation into the effect of core hardening upon the degree of core compression reveals that for the practical choice $\bar{m} = 1.0$, the level of hardening has little effect upon the nominal core compression strain ε_c: the ideally plastic shock wave model of Section 2.1.2 suffices to predict the dynamic compression of sandwich cores.

3. Fluid–structure interaction in sandwich plates

In his pioneering paper, Taylor (1941) computed the momentum transmitted to a free-standing plate due to the impingement of a one-dimensional shock wave. Fleck

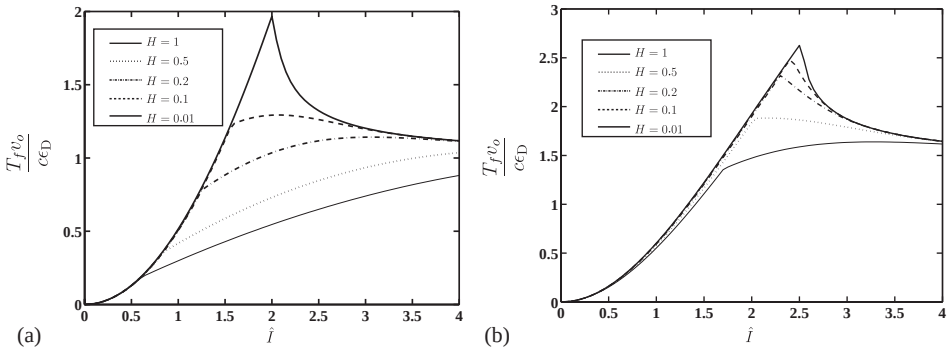

Fig. 6. Core compression time as a function of the shock impulse for selected values of the core hardening rate H. Results are shown for core to face sheet mass ratios (a) $\bar{m} = 0.1$ and (b) $\bar{m} = 1.0$.

and Deshpande (2004) followed this approach and computed the momentum transmitted to a sandwich plate by treating the outer face of the sandwich plate as a free-standing plate without support of the core during this fluid–structure interaction phase. We proceed to develop finite element and lumped parameter models to explore the accuracy of this assumption and determine the regimes in which the analysis of Fleck and Deshpande (2004) is valid.

3.1. Summary of the Taylor model for a free standing plate

We begin by reviewing briefly the Taylor (1941) model for a plane wave impinging an infinite, free-standing rigid plate at normal incidence. Consider an incoming acoustic wave in a fluid of density ρ_w, travelling with a constant velocity c_w in the direction of increasing x measured along the inward normal to the plate. The origin is taken at the front of the plate and the transverse deflection of the plate is written as $w(t)$ in terms of time, t. Upon making the usual assumption that the pressure profile for the incoming shock wave can be taken to be a decaying exponential in shape, with time constant θ, the incoming pressure wave is written as

$$p_I(x,t) = p_0 \mathrm{e}^{-(t-x/c_w)/\theta}, \tag{22}$$

If the front face were rigid and fixed in space, the reflected wave would read

$$p_{r1}(x,t) = p_0 \mathrm{e}^{-(t+x/c_w)/\theta}, \tag{23}$$

corresponding to perfect reflection of the wave, travelling in the $-x$ direction. But the front face sheet is not fixed: it accelerates as a rigid body with a mass per unit area m_f, and moves with a velocity $\dot{w}(t)$. Consequently, the fluid elements adjacent to the front face possess the common velocity $\dot{w}(t)$, and a rarefaction wave p_{r2}, of magnitude

$$p_{r2}(x,t) = -\rho_w c_w \dot{w}\left(t + \frac{x}{c_w}\right), \tag{24}$$

is radiated back into the fluid from the front face. Thus, the net water pressure $p(x,t)$ due to the incoming and reflected waves is

$$p(x,t) = p_I + p_{r1} + p_{r2} = p_0[e^{(-(t-x/c_w)/\theta} + e^{-(t+x/c_w)/\theta}] - \rho_w c_w \dot{w}\left(t + \frac{x}{c_w}\right). \quad (25)$$

This relation only holds when the pressure p is much less than the bulk modulus $E_w \equiv c_w^2 \rho_w$ of the fluid. The front face of the sandwich plate (at $x = 0$) is accelerated by the net pressure acting on it, giving the ordinary differential equation governing the face motion as

$$m_f \ddot{w} + \rho_w c_w \dot{w} = 2p_0 e^{-t/\theta}. \quad (26)$$

Upon imposing the initial conditions $w(0) = \dot{w}(0) = 0$, and introducing the non-dimensional measure $\psi \equiv \rho_w c_w \theta / m_f$, the solution of (26) is

$$w(t) = \frac{2p_0\theta^2}{m_f(\psi - 1)\psi}[(\psi - 1) + e^{-\psi t/\theta} - \psi e^{-t/\theta}]. \quad (27)$$

The pressure distribution follows immediately from (25). In particular, the pressure on the front face is

$$p(t, x = 0) = 2p_0 e^{-t/\theta} - \frac{2p_0\psi}{\psi - 1}[e^{-t/\theta} - e^{-\psi t/\theta}]. \quad (28)$$

For the case of a liquid containing dissolved gases, the pressure loading on the front face ceases and the liquid cavitates when $p(t, x = 0) \to 0$, thereby defining the cavitation time τ_c. Substitution of this condition into (28) provides the simple relation

$$\frac{\tau_c}{\theta} = \frac{1}{\psi - 1} \ln \psi. \quad (29)$$

The net impulse conveyed to the face follows from (27) as

$$I_t = \zeta I_0, \quad (30)$$

in terms of the maximum achievable impulse I_0 (achieved in the stationary plate limit),

$$I_0 = \int_0^\infty 2p_0 e^{-t/\theta}\, dt = 2p_0\theta, \quad (31a)$$

and in terms of the knock-down factor

$$\zeta \equiv \psi^{-(\psi/\psi - 1)}. \quad (31b)$$

3.2. Finite element (FE) analysis

The Taylor model assumes that the front face behaves as a free standing plate, decoupled from the core and the rear face sheet. It is instructive to relax this

simplifying assumption and to include in the model the dynamic response of the core and the rear face sheet of the sandwich plate.

A finite element scheme is now developed in order to model the full 1D fluid–structure interaction problem, for an incoming shock wave in the fluid, and the ensuing wave propagation within the fluid and within each layer of the sandwich plate. The FE method is a convenient technique as it is able to handle:

(i) fluid–structure interaction after first cavitation,
(ii) multiple wave reflections within the faces, and
(iii) the non-linear dynamic response of the core.

An updated Lagrangian scheme is employed with the current configuration at time t serving as the reference. The co-ordinate x denotes the position of a material point in the current configuration with respect to a fixed Cartesian frame, and u is the displacement of that material point. For the one-dimensional problem under consideration, the principle of virtual work (neglecting effects of gravity) for a volume V and surface S is written in the form

$$\int_V \sigma \delta\varepsilon \, \mathrm{d}V = \int_S T \delta u \, \mathrm{d}S - \int_V \rho \frac{\partial^2 u}{\partial t^2} \, \delta u \, \mathrm{d}V, \tag{32}$$

where σ is the Cauchy stress, $\varepsilon \equiv \partial u/\partial x$ is the strain, T is the traction on the surface S of the current configuration and ρ is the material density in the current configuration.

A finite element discretisation based on linear, one-dimensional elements is employed. When the finite element discretisation of the displacement field is substituted into the principle of virtual work (32) and the integrations are carried out, the discretised equations of motion are obtained as

$$\mathbf{M} \frac{\partial^2 \mathbf{U}}{\partial t^2} = \mathbf{R}, \tag{33}$$

where $\mathbf{U}$ is the vector of nodal displacements, $\mathbf{M}$ is the mass matrix and $\mathbf{R}$ is the nodal force vector. A lumped mass matrix is used in (33) instead of a consistent mass matrix, since this is preferable for explicit time integration procedures, for both accuracy and computational efficiency (Krieg and Key, 1973). An explicit time integration scheme, based on the Newmark β-method with $\beta = 0$, is used to integrate (33) to obtain the nodal velocities and displacements, see Xu and Needleman (1994) for further details. Typically, there are 40,000 elements in the fluid, 2000 in the core and 200 in each face sheet.

3.2.1. Material properties

Consider a sandwich plate of infinite extent with identical face sheets of thickness h and a core of thickness c, as shown in Fig. 7. The face sheets of the sandwich plate are assumed to be made from an elastic solid with Young's modulus E_f and density ρ_f. The core is modelled as an elastic–plastic rate dependent solid with the total logarithmic strain rate $\dot{\varepsilon}$ written as the sum of an elastic logarithmic strain rate $\dot{\varepsilon}^{\mathrm{e}}$ and

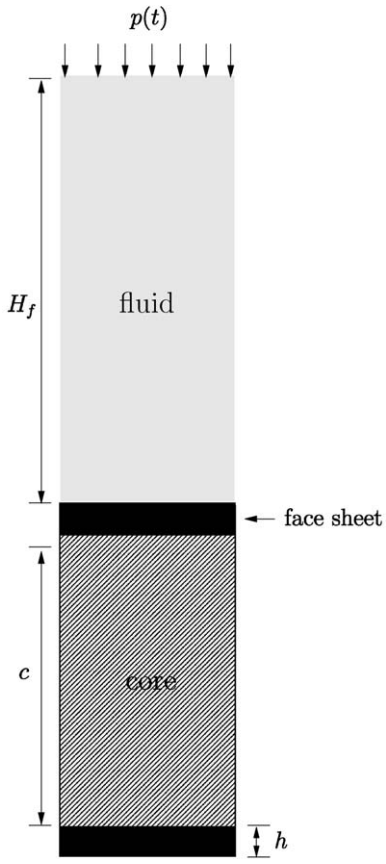

Fig. 7. Boundary value problem analysed in the one-dimensional finite element fluid–structure interaction simulations.

a plastic logarithmic strain rate $\dot{\varepsilon}^{\mathrm{p}}$, so that at the stress level σ

$$\dot{\varepsilon} = \dot{\varepsilon}^{\mathrm{e}} + \dot{\varepsilon}^{\mathrm{p}}\,\mathrm{sign}\,(\sigma). \tag{34a}$$

The elastic strain rate is related to the stress rate by

$$\dot{\varepsilon}^{\mathrm{e}} = \frac{\dot{\sigma}}{E_c}, \tag{34b}$$

in terms of the Young's modulus E_c of the core. An overstress viscoplastic model is taken for the plastic strain rate,

$$\dot{\varepsilon}^{\mathrm{p}} = \begin{cases} \left(\dfrac{|\sigma| - \sigma_c}{\eta}\right) & \text{if } \varepsilon^{\mathrm{p}} < -\ln(1-\varepsilon_D)\ \&\ |\sigma| > \sigma_c, \\ 0 & \text{otherwise,} \end{cases} \tag{34c}$$

where σ_c is the yield strength, η is the viscosity and ε_D is the nominal densification strain (taken to be positive). A prescription for the value of viscosity η and mesh size

in the FE calculations is given in Appendix A. Following Bleich and Sandler (1970), the fluid medium is modelled as a bilinear elastic solid with density ρ_w. In particular, the stress σ versus logarithmic strain ε relationship is taken to be

$$\sigma = \begin{cases} E_w \varepsilon & \varepsilon \leqslant 0 \\ 0 & \varepsilon > 0, \end{cases} \tag{35}$$

so that the fluid is assumed to be incapable of sustaining tensile loading.

Unless otherwise specified, the reference sandwich plate comprises steel face sheets and a compressible steel core of relative density 10%, representative of that for metallic foams and multi-layer lattice materials. The face sheets are assumed to be of thickness $h = 10\,\text{mm}$ and made from an elastic solid of Young's modulus $E_f = 210\,\text{GPa}$ and density $\rho_f = 8000\,\text{kg m}^{-3}$. The core is of thickness $c = 100\,\text{mm}$, of density $\rho_c = 800\,\text{kg m}^{-3}$, and has a nominal densification strain $\varepsilon_D = 0.5$; it has a yield strength σ_c in the range 0.4–50 MPa, a Young's modulus of $E_c = 1000\sigma_c$ and a viscosity $\eta = 1.0\,\text{kPas}$ (see Appendix A). The reference material properties of the fluid medium are $\rho_w = 1.0\,\text{Mg m}^{-3}$ and $E_w = 1.96\,\text{GPa}$, giving a wave speed $c_w = 1400\,\text{m s}^{-1}$, representative of that for water.

3.2.2. Boundary conditions

The one-dimensional problem considered is sketched in Fig. 7; it comprises a free-standing sandwich plate, with a column of fluid of height H_f. A pressure history

$$p = p_0 \mathrm{e}^{-t'/\theta}, \tag{36}$$

is applied to the top of the fluid column as shown in Fig. 7. Here, the time t' is measured from the instant of application of the pressure to the top of the fluid column. In contrast, the time t is measured from the instant that the shock wave impinges on the structure. The two are related by $t' = t + (H_f/c_w)$. Unless otherwise stated, the reference shock wave properties are $p_0 = 100\,\text{MPa}$ and $\theta = 0.1\,\text{m s}$. In all calculations reported here, the height H_f of the water column is taken to be sufficiently large that the reflected wave does not reach the top of the water column over the duration of the calculations reported. Thus, the column can be considered to be semi-infinite in extent.

3.2.3. Numerical results

Calculations are presented in this section for the case of the reference shock wave impinging the sandwich plate. The effect of the core strength σ_c is explored by considering three values of σ_c, with all other sandwich plate properties kept fixed at their reference values.

The progressive increase in normalised momentum I/I_0 of the entire sandwich plate with increasing normalised time t/θ, as measured from the instant of the shock wave impinging on the structure, is plotted in Fig. 8a for the selected values of core strength $\bar{\sigma} \equiv \sigma_c/p_0 = 0.004$, 0.105 and 0.525. The sandwich plate of core strength $\bar{\sigma} = 0.525$ acquires a sharp increase in momentum during $0 < t/\theta < 1.5$. Thereafter, the momentum remains constant indicating separation of the sandwich plate from

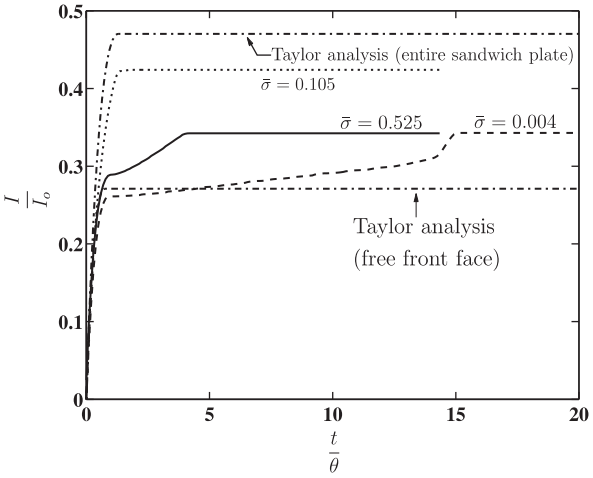

Fig. 8. Finite element and Taylor predictions of the momentum of the sandwich plate. Results are shown for selected values of the core strength $\bar{\sigma}$ with all other material properties equal to the reference values.

the fluid. In contrast, the sandwich plate of core strength $\bar{\sigma} = 0.105$ shows a sharp increase in momentum up to $t/\theta \approx 1.0$, followed by a more gradual increase up to $t/\theta \approx 4.2$. At later times, the momentum remains constant. Similarly, the momentum of the sandwich plate of core strength $\bar{\sigma} = 0.004$ initially rises rapidly and then more gradually for $t/\theta > 1.0$. Unlike the $\bar{\sigma} = 0.105$ sandwich plate, the momentum of the $\bar{\sigma} = 0.004$ sandwich plate again rises sharply at $t/\theta \approx 15$ before flattening out. Overall, the $\bar{\sigma} = 0.004$ and 0.105 sandwich plates acquire approximately equal amounts of momentum, while a larger fraction of the shock impulse is transferred to the $\bar{\sigma} = 0.525$ sandwich plate.

The Taylor analysis assuming a free-standing front face of the sandwich plate gives $I/I_0 = 0.27$ and this result is included in Fig. 8. An alternative Taylor-type calculation can be performed assuming the whole sandwich plate behaves as a rigid, free-standing mass during the shock event. Then, the increased mass of the plate compared to that of the front face leads to an increased value of transmitted impulse, $I/I_0 = 0.47$. The detailed FE calculations give values of I/I_0 which are bounded by the Taylor estimate $I/I_0 = 0.47$ for a rigid sandwich plate, and the Taylor estimate $I/I_0 = 0.27$ for a free standing front plate.

The pressure versus time history at the interface between the fluid and the sandwich plate is shown in Fig. 9a for $0 < t/\theta < 2.0$ and in Fig. 9b for, $0 < t/\theta < 20$, for the cases discussed above. In all cases the peak pressure $p_{\max}$ at $t = 0$ is given by

$$p_{\max} = \frac{2\sqrt{\rho_f E_f}}{\sqrt{\rho_f E_f} + \sqrt{\rho_w E_w}} p_0 \approx 1.93 p_0. \tag{37}$$

Note that the y-axis of Fig. 9b has been truncated at $p/p_0 = 0.2$ for the sake of clarity. For normalised times t/θ less than approximately 1.5, the pressure at the

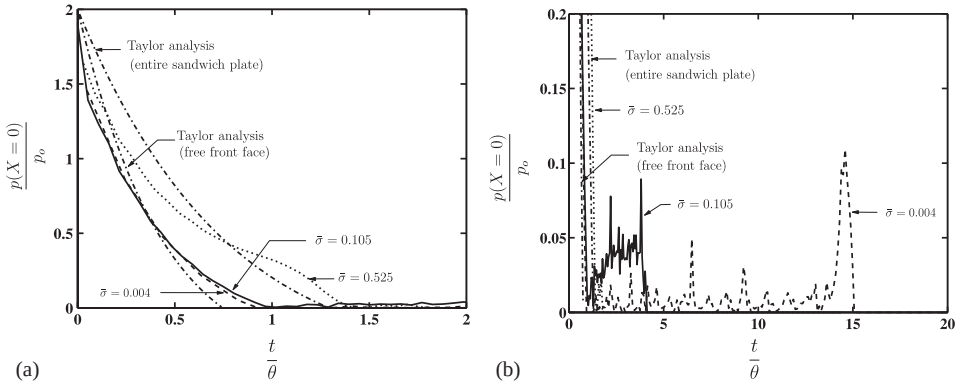

Fig. 9. Finite element and Taylor predictions of the fluid pressure on the front face as a function of time. (a) early time history and (b) time history to the end of the fluid loading. Results are shown for selected values of the core strength $\bar{\sigma}$ with all other material properties equal to the reference values.

interface drops rapidly with time in all cases, see Fig. 9a. Recall that the Taylor analyses neglect elasticity within the faces, and predict $p_{\max} = 2p_0$, whereas the more accurate elastic description (37) gives $p_{\max} \approx 1.93p_0$. Consequently, the two Taylor analyses do not bound the pressure versus time history at short times $t/\theta < 2.0$. In both Taylor analyses and for the sandwich plate with $\bar{\sigma} = 0.525$, the pressure at the interface drops to zero and then does not rise again. On the other hand, for the sandwich plates of $\bar{\sigma} = 0.105$ and 0.004 the interfacial pressure remains positive up to $t/\theta \approx 4.0$ and 15, respectively, and this finite pressure results in a gradual increase in the momentum of these plates with time. Moreover, a spike in the pressure at $t/\theta \approx 15$ for the $\bar{\sigma} = 0.004$ sandwich plate results in the sharp increase in momentum of that sandwich plate at $t/\theta \approx 15$, recall Fig. 8a.

The time evolution of normalised average velocities v_f/v_0 and v_b/v_0 of the front and rear faces, respectively, are plotted in Fig. 10a. Here, the velocities have been normalised by $v_0 = I_0/m_f$, where m_f is the mass per unit area of the face sheets. For the sandwich plates with the two weaker cores, the velocities of the front face sheets increase rapidly with time, followed by an extended period over which the front face sheet decelerates while the rear face accelerates until both face sheets acquire the same velocity. After this, only elastic vibrations of the face sheets are observed. On the other hand, for the sandwich plate with $\bar{\sigma} = 0.525$, there is no distinct phase over which the front face decelerates and the rear face accelerates, indicating that this sandwich plate behaves almost like a monolithic plate. For all sandwich plates considered, complete separation of the sandwich plate from the fluid always occurs when the velocities of the face sheets equalise. This is evidenced by the fact that the momentum attains its final value, when the velocities of faces equalise, compare Figs. 8 and 10a. The average nominal core compression strain ε_c is plotted in Fig. 10b as a function of time. The degree of core compression increases with decreasing $\bar{\sigma}$, and for the weakest core, $\bar{\sigma} = 0.004$,

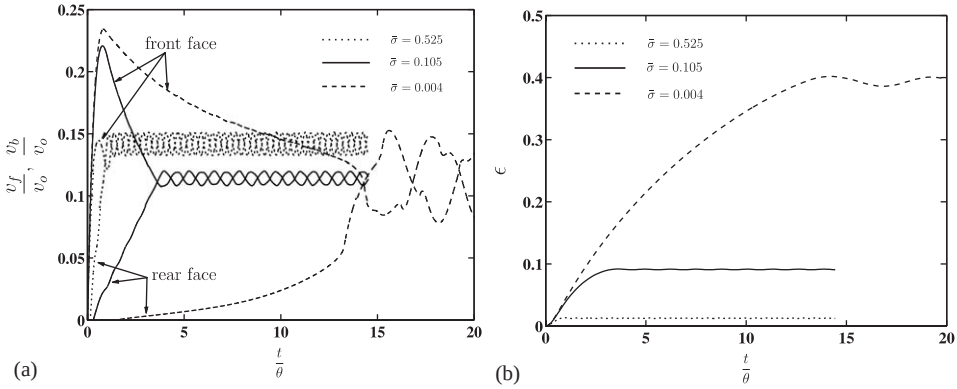

Fig. 10. Finite element predictions of (a) the front and rear face sheet velocities and (b) core compression ε as a function of time. Results are shown for selected values of the core strength $\bar{\sigma}$ with all other material properties equal to the reference values.

densification[2] occurs at $t/\theta \approx 15$. At this instant the core locks up and the front and face faces acquire the same velocity almost instantaneously. The rapid drop in front face velocity sends a compressive spike in pressure back into the fluid, see Fig. 10b.

The spatial variation of pressure in the fluid at selected times $t/\theta = 0.91$, 1.0 and 1.39 is plotted in Fig. 11a for the sandwich plate of intermediate strength $\bar{\sigma} = 0.105$. Here, X is the spatial co-ordinate in the undeformed configuration with $X = 0$ corresponding to the fluid–structure interface. (The pressure at $X = 0$ has already been presented in Fig. 9.) At time $t/\theta = 0.91$, the pressure is positive everywhere in the fluid, and the reflected wave has reached the location $X/(c_w\theta) \approx -0.93$. Subsequently, the fluid cavitates at $X/(c_w\theta) \approx -0.1$ and a breaking front travels supersonically both away from and towards the structure, with widening of the cavitation zone such that at $t/\theta = 1.0$ it extends from $X/(c_w\theta) = -0.3$ to -0.04. The spatial variation of the nominal strain ε_w in the fluid at the three selected times is plotted in Fig. 11b. The time $t/\theta = 0.91$ is prior to cavitation and ε_w everywhere is compressive. In contrast, at $t/\theta = 1.0$ and 1.39, ε_w is tensile within the cavitated region. The magnitude of the tensile strain is sufficiently low (<2 %) that the density of the fluid in the cavitated region is approximately equal to that of the uncavitated fluid, indicating that the cavitated fluid contains a dilute suspension of air bubbles rather than existing as water vapour. At a time t/θ between 1.0 and 1.39, the cavitated fluid near the structure ($0 < X < 0.1c_w\theta$) begins to reconstitute and the pressure near the fluid–structure interface rises again (compare the pressure distributions at $t/\theta = 1.0$ and 1.39 in Fig. 11). However, the other breaking front continues to travel supersonically away from the structure as seen from the pressure distribution at $t/\theta = 1.39$. These findings are consistent with those reported in Kennard (1943)and Bleich and Sandler (1970). Analytical calculations for a shock

[2]The FE calculations assume a shock wave of finite width (on the order of 5 mm), see Appendix A. Consequently, the core locks up at ε_c slightly less than ε_D. Whilst it would be attractive to reduce the width of the shock front, this would necessitate a much finer mesh.

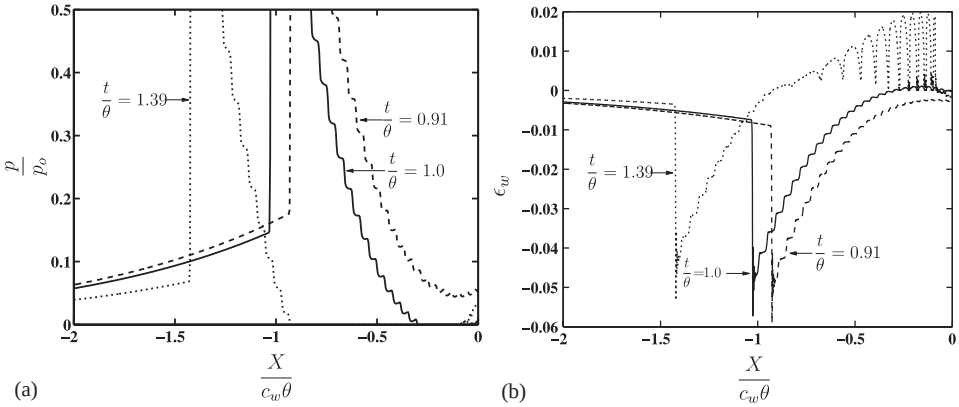

Fig. 11. (a) Fluid pressure p and (b) nominal strain ε_w in the fluid as a function of the distance from the front face sheet for shock loading (with reference shock properties) of a sandwich plate with reference material properties and $\bar{\sigma} = 0.105$. The distributions are shown for three selected values of time t/θ.

wave impinging a plate on an elastic foundation by Temperley (1950) support the notion that clean separation does not occur at the plane of first cavitation.

3.3. *A lumped parameter model for a sandwich plate with a compressible rigid, plastic core*

The underwater shock problem involves a wide range of length scales from the size of the structure to the decay length of the incident wave. Commonly used numerical schemes (such as the total wave formulation in FE codes) require extreme mesh refinement in the fluid to reduce the "numerical" dispersion on the incoming shock wave. Thus, an accurate analysis of the fluid–structure interaction problem in realistic structures is prohibitively time consuming, as discussed by Sprague (2002). Simple analytical models for the fluid–structure interaction problem have applications in not only structural optimisation studies such as those carried out recently by Fleck and Deshpande (2004) and Hutchinson and Xue (2005), but also give physical insight and serve as useful guidelines in the initial design stages of underwater structures.

We proceed to develop a simplified one-dimensional shock wave analysis of the shock response of a sandwich plate. A lumped parameter approach is adopted to calculate the velocity of the front and back face sheet as a function of time: each face sheet is treated as rigid, and of mass m_f per unit area. Shock propagation within the fluid up to the point of first cavitation is handled as before, with the incoming shock wave specified by (22) and the fluid treated as a linear elastic medium of density ρ_w and elastic speed c_w. The calculation is terminated at the onset of first cavitation, as the response of the fluid then becomes non-linear. The core of the sandwich plate comprises a rigid, ideally plastic solid of strength σ_c with a nominal densification strain ε_D as in Section 2.1.2. Since each face is a rigid body, the thickness of each face does not enter the calculation, and the origin is taken as the front face of the

sandwich plate. The co-ordinate x in the deformed configuration is taken along the inward normal to the plate, with the fluid occupying $x \leqslant 0$. By neglecting the elasticity of the faces and core of the sandwich plate, we obtain a coupled set of ordinary differential equations for the sandwich plate. In contrast, the numerically intense finite element method is needed to handle elastic wave propagation within each layer of the sandwich plate, and the post cavitation response of the fluid. These finite element calculations solve a coupled set of partial differential equations and are too time consuming to investigate the response of sandwich plates over a wide range of parameters, as will be seen subsequently.

Consider an incoming wave in the fluid, travelling with a constant velocity c_w in the direction of increasing x. Upon neglecting elastic wave propagation effects in the core two distinct cases arise: (i) a plastic shock wave propagates in the core, and (ii) no plastic shock wave propagates within the core. We consider each case in turn and then derive the conditions for their applicability.

3.3.1. Governing equations for plastic shock wave propagation in the core

Assume that a plastic shock wave travels in the core from the front to the rear face sheet, at a wave speed $c_{\rm pl}(t)$. At time t, the plastic shock wave has travelled a distance X through the foam core (undeformed configuration); the front face sheet and adjacent foam downstream from the shock wave share the velocity v_d. Similarly, the foam upstream from the shock and the rear face sheet share a common velocity v_u. At any instant the foam is non-deforming except for a jump in compressive nominal strain of magnitude ε_D across the shock wave. Associated with this strain jump is a stress jump: σ_d is the stress on the downstream face of the shock wave and, as discussed in Section 2.1.2, the foam is at incipient yield on the upstream face of the shock wave. Consequently, the equations of motion of the sandwich plate at time t are

$$2p_0 \mathrm{e}^{-t/\theta} - \rho_w c_w v_u - \sigma_d = \left(m_f + m_c \frac{X}{c}\right)\dot{v}_d, \tag{38a}$$

and

$$\left[m_f + m_c\left(1 - \frac{X}{c}\right)\right]\dot{v}_u = \sigma_c, \tag{38b}$$

while conservation of momentum and mass across the shock wave dictates that

$$\sigma_d - \sigma_c = \frac{m_c}{c}\, c_{\rm pl}(v_d - v_u), \tag{39a}$$

and

$$\dot{X} = c_{\rm pl} = \frac{v_d - v_u}{\varepsilon_D}, \tag{39b}$$

respectively. Define the maximum achievable impulse at $I_0 = 2p_0\theta$ and introduce the non-dimensional groups

$$\bar{I} \equiv \frac{I_0\theta}{m_f c \varepsilon_D} \quad \text{and} \quad \psi \equiv \frac{\rho_w c_w \theta}{m_f}, \tag{40}$$

to characterise the loading, and

$$\bar{\sigma} \equiv \frac{\sigma_c}{p_0} \quad \text{and} \quad \bar{m} \equiv \frac{m_c}{m_f} \tag{41}$$

to characterise the core properties. Upon writing the non-dimensional time as $\bar{t} \equiv t/\theta$ and the non-dimensional velocities as $\bar{v}_d \equiv v_d m_f/I_0$ and $\bar{v}_u \equiv v_u m_f/I_0$, the above equations of motion are given in non-dimensional form as

$$e^{-\bar{t}} - \psi \bar{v}_u - \frac{\bar{\sigma}}{2} - \bar{m}\bar{I}(\bar{v}_d - \bar{v}_u)^2 = (1 + \bar{m}\bar{s})\dot{\bar{v}}_d, \tag{42a}$$

$$\frac{\bar{\sigma}}{2} = [1 + \bar{m}(1 - \bar{s})]\dot{\bar{v}}_u, \tag{42b}$$

$$\dot{\bar{X}} = \bar{I}(\bar{v}_d - \bar{v}_u), \tag{42c}$$

where $\bar{X} \equiv X/c$. Eqs. (42) are valid for a core which is sufficiently weak that a plastic shock wave initiates within the core. Employing the condition that at $t = 0$, $\dot{v}_d > \dot{v}_u$, the governing relations (42) require

$$\frac{\bar{\sigma}}{2} < \frac{1 + \bar{m}}{2 + \bar{m}}. \tag{42d}$$

The above set of ordinary differential equations with initial conditions $\bar{v}_u = \bar{v}_d = \bar{s} = 0$ at $\bar{t} = 0$ is solved numerically[3] to obtain the momentum

$$\frac{I}{I_0} \equiv (1 + \bar{m}\bar{s})\bar{v}_d + [1 + \bar{m}(1 - \bar{s})]\bar{v}_u, \tag{43}$$

of the sandwich plate as a function of time. The above equations of motion are valid until one of the following events occur:

Event (i). Cavitation occurs within the fluid. Assuming that the fluid can sustain no tension, cavitation occurs when the pressure anywhere in the fluid first becomes negative:

$$p(x, t)/p_0 = [e^{-\bar{t}+\bar{x}} + e^{-\bar{t}-\bar{x}}] - 2\psi\bar{v}_d(\bar{t} + \bar{x}) \to 0^-, \tag{44}$$

for any $\bar{x} \equiv x/(c_w\theta) \leqslant 0$. The overall calculation is terminated if this event is triggered.

Event (ii). The shock wave reaches the rear face sheet, i.e. $\bar{X} \to 1$.
Event (iii). The shock wave arrests within the core $\dot{\bar{X}} \to 0$.

At the instant of first cavitation, i.e. $p(x_c, t_c) = 0$, the momentum of the sandwich plate is given by (43), while the momentum I_w of the fluid trapped between the

[3]The MATLAB function *ode23* based on an automatic step-size Runge–Kutta–Fehlberg integration method was employed to solve (42).

cavitation plane at $x_c < 0$ and the front face of the sandwich plate ($x = 0$) is given by

$$\frac{I_w}{I_0} = \frac{1}{2}\int_{\bar{x}_c}^{0} [e^{-\bar{t}_c+\bar{x}} - e^{-\bar{t}_c-\bar{x}} + 2\psi\bar{v}_u(\bar{t}_c + \bar{x})]\,d\bar{x}. \tag{45}$$

Here, $\bar{x}_c \equiv x_c/(c_w\theta)$ and $\bar{t}_c \equiv t_c/\theta$ is the non-dimensional cavitation time.

3.3.2. Governing equations involving no shock wave propagation in the core

The sandwich plate behaves as a monolithic plate of mass $2m_f + m_c$ when no shock wave is propagating within the core. The governing equations of the motion then switch from (42) to

$$e^{-\bar{t}} - 2\psi\bar{v} = (2 + \bar{m})\dot{\bar{v}}, \tag{46}$$

in terms of the non-dimensional velocity of the sandwich plate $\bar{v} \equiv vm_f/I_0$. The initial conditions for (46) are set by one of the two following cases.

Initial condition (a) If the core is sufficiently strong that (42d) is not satisfied, then no shock wave initiates within the core. The appropriate initial conditions for (46) are $\bar{v} = 0$ at $\bar{t} = 0$. The sandwich plate analysis reduces to the Taylor free-standing plate analysis but based on the areal mass of the full sandwich plate (Section 3.1), with ψ replaced by $\psi/(2 + \bar{m})$.

Initial condition (b) In prior history, a shock wave has initiated and propagated within the core, but has just arrested by either events (ii) or (iii) of Section 3.3.1. If the shock wave has just reached the rear face sheet (event (ii)), it is assumed that the inelastic impact of the combined rigid front face sheet and core against the rigid rear face sheet equalises the velocities instantly. Then, conservation of momentum dictates that the initial condition for (46) is

$$\bar{v} = \frac{(1 + \bar{m})\bar{v}_d + \bar{v}_u}{2 + \bar{m}}, \tag{47}$$

at time $\bar{t} = \bar{t}_e$, where $\bar{t}_e$ is the time at which the shock wave has reached the rear face sheet, and $\bar{v}_u$ and $\bar{v}_d$ are the velocities at time $\bar{t}_e$ as given by the analysis of Section 3.3.1. If the shock wave has arrested within the core (event (iii)), the initial condition for (46) is given by $\bar{v} = \bar{v}_u = \bar{v}_d$ at time $\bar{t} = \bar{t}_e$, where $\bar{t}_e$ is the time at which the shock wave has arrested in the core.

The pressure in the fluid is again given by (44) with $\bar{v}_d$ replaced by $\bar{v}$. It is emphasised that the time integration procedure for (42) or (46) continues until first cavitation. The main quantities recorded are the momentum of the sandwich plate (via (43)), the location of the cavitation plane x_c (via (44)) and the momentum of the trapped fluid at $x_c \leqslant X \leqslant 0$, via (45). The lumped parameter model is not employed to predict the average core compression strain ε_c as negligible core compression occurs up to the

instant of first cavitation and the model is not sufficiently sophisticated to capture the post cavitation fluid–structure interactions.

A simplified model, that is based on a perturbation to the Taylor analysis, and is accurate for small values of $\bar{\sigma}$, is presented in Appendix B.

3.3.3. *Fluid–structure interaction map*

The regimes of behaviour predicted by the above lumped parameter shock model can be summarised in a fluid–structure interaction map. Consider a sandwich plate with $\bar{m} = 1.0$ and subjected to a shock impulse of magnitude $\bar{I} = 0.5$. A fluid–structure interaction map with axes of non-dimensional core strength $\bar{\sigma}$ and the Taylor fluid–structure interaction parameter ψ is plotted in Fig. 12. Included in the map are contours of the normalised momentum I_t/I_0 of the sandwich plate at the instant of first cavitation in the fluid together with the location $x_c/(c_w\theta)$ of first cavitation. Four distinct regimes of behaviour are marked on the map (and are also summarised in Table 1):

(i) Regime I: the plastic shock wave in the core reaches the rear face sheet before cavitation occurs in the fluid.
(ii) Regime II: the fluid cavitates before the plastic shock wave has arrested in the core.
(iii) Regime III: the plastic shock wave arrests in the core before cavitation.
(iv) Regime IV: the plastic shock wave does not initiate in the core.

It is evident from the map that a larger fraction of the shock impulse is transmitted into the plate with decreasing values of ψ; this is consistent with the Taylor prediction for a free-standing monolithic plate. For any given value of ψ, I_t/I_0

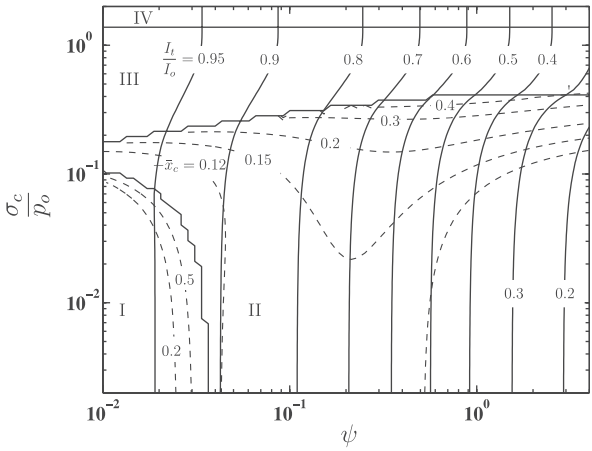

Fig. 12. Fluid structure interaction map ($\bar{I} = 0.5, \bar{m} = 1.0$) with axes of core strength σ_c/p_0 and the Taylor fluid–structure interaction parameter ψ. The four regimes of behaviour are marked on the map. Contours of the impulse transmitted into the sandwich plate at first cavitation and the distance of that cavitation plane from the front face of the sandwich plate are also included.

Table 1
The four regimes of characterising the fluid–structure interaction behaviour of sandwich plates

Sequence of response	$\varepsilon_c = 0$	$\varepsilon_c < \varepsilon_D$ at cavitation	$\varepsilon_c = \varepsilon_D$
Cavitation before completion of core compression	—	Regime II ($\bar{x}_c < 0$)	
Cavitation after completion of core compression	—	Regime III ($\bar{x}_c = 0$)	Regime I ($\bar{x}_c \leqslant 0$)
No core compression (monolithic plate response)	Regime IV	—	—

increases with increasing core strength $\bar{\sigma}$, with the main increase occurring at the transition between regimes II and III. The contours of $x_c/(c_w\theta)$ indicate that cavitation occurs within the fluid in regimes I and II while cavitation occurs at the fluid–structure interface in regimes III and IV. Note that the cavitation location changes in a non-monotonic manner with increasing $\bar{\sigma}$: the cavitation plane moves away from the front face of the sandwich plate with increasing $\bar{\sigma}$ in regime II, but occurs at the fluid–structure interface in regime III. This discontinuity in x_c across the regime II–III boundary arises from the fact that the model neglects elastic wave effects in the core; the model predicts that the resistive pressure by the core on the front face of the sandwich plate changes discontinuously from σ_c to 0 across the regime II–III boundary, at cavitation.

The fluid–structure interaction map for a larger impulse $\bar{I} = 5.0$ ($\bar{m} = 1.0$) is plotted in Fig. 13. In contrast to the $\bar{I} = 0.5$ map in Fig. 12, regime I now dominates the map, with complete core densification occurring for most realistic values of ψ and $\bar{\sigma}$ due to the higher shock impulse. The transmitted impulse I_t/I_0 is almost constant across the regime I and III boundary for any given value of ψ. This is rationalised by recalling that in both regimes I and III cavitation occurs after arrest of the shock wave in the core, and thus the momentum transmitted into the sandwich plate is primarily a function of the total plate mass $2m_f + m_c$ in both regimes I and III.

3.4. Parametric study, and a comparison between FE and the lumped parameter model

We proceed to present a parametric study to investigate the dependence of the shock momentum transmitted into the sandwich plate as a function of the core strength $\bar{\sigma}$, the shock impulse $\bar{I}$, the core mass $\bar{m}$ and the Taylor fluid–structure interaction parameter ψ. Predictions are given for both the FE and lumped parameter models. The lumped parameter model is dependent upon the following non-dimensional groups: $\bar{I} \equiv I_0\theta/(m_f c\varepsilon_D)$, $\psi \equiv \rho_w c_w \theta/m_f$, $\bar{\sigma} \equiv \sigma_c/p_0$ and $\bar{m} \equiv m_c/m_f$. The FE analysis makes use of these groups and the additional non-dimensional groups: h/c, p_0/E_w, σ_c/E_c, E_w/E_f and η/I_0. In the FE calculations these additional groups have been set set to a value $\leqslant 0.1$; numerical experimentation confirmed that the FE solution is insensitive to the value of these additional groups provided they are less than 0.1. Only a limited set of comparisons between the FE and lumped parameter model predictions are presented: the height H_f of the fluid

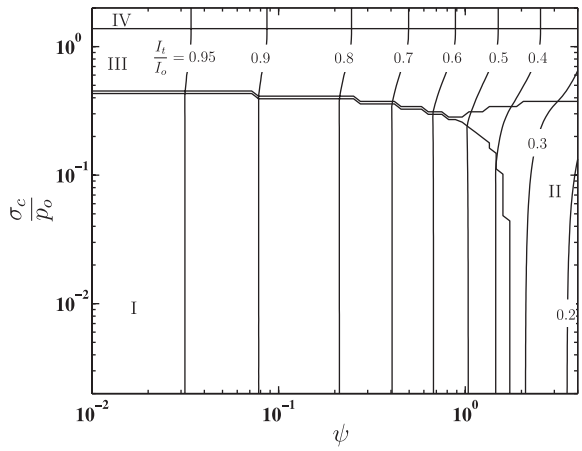

Fig. 13. Fluid structure interaction map ($\bar{I} = 5.0$, $\bar{m} = 1.0$) with axes of core strength σ_c/p_0 and the Taylor fluid–structure interaction parameter ψ. The four regimes of behaviour are marked on the map. Contours of the ratio of the impulse transmitted into the sandwich plate at first cavitation are also included.

column required in the FE calculations scales as $\bar{I}E_w/(\psi p_0)$ and thus for a fixed p_0/E_w the height, H_f increases with decreasing ψ. This makes the FE calculations prohibitively time consuming for small ψ.

In our parametric study using both the FE and lumped parameter models first consider the effect of core strength, with all other sandwich plate and shock wave properties held fixed at their reference values: we vary $\bar{\sigma}$ with $\bar{I} = 0.5$, $\bar{m} = 1.0$ and $\psi = 1.75$. Finite element predictions of both the momentum of the sandwich plate at the instant of first cavitation (the first knee in the momentum versus time curves, see Fig. 8a) and the final momentum of the sandwich plate are plotted in Fig. 14a as a function of $\bar{\sigma}$. As discussed in Section 3.3, the lumped parameter model cannot be employed to predict ε_c and thus only FE predictions are plotted in Fig. 14b. At $\bar{\sigma} \equiv \sigma_c/p_0 < 0.01$ full densification occurs while at higher $\bar{\sigma}$ the core only partially densifies. For $\bar{\sigma}$ greater than approximately 0.2, the momentum at first cavitation is approximately equal to the final momentum, while for lower values of $\bar{\sigma}$, the final momentum is considerably higher than the momentum at first cavitation. It is also evident that a larger fraction of the shock impulse is transmitted into the sandwich plate for higher values of $\bar{\sigma}$. Both observations are rationalised by noting that for high values of $\bar{\sigma}$, the degree of core compression is small (Fig. 14b) and the sandwich plate behaves essentially as a monolithic plate; cavitation occurs at the fluid–structure interface, with no subsequent interaction between the fluid and the sandwich plate.

Two sets of predictions by the lumped parameter model for the momentum transmitted into sandwich plate are included in Fig. 14a: (i) the solid line is the prediction of the momentum transmitted into the sandwich plate at first cavitation and (ii) the dashed line is the sum of the momentum of the sandwich plate at first cavitation and the momentum I_w trapped in the fluid between the cavitation plane and the front face of the sandwich plate. As already noted in Fig. 12, the lumped

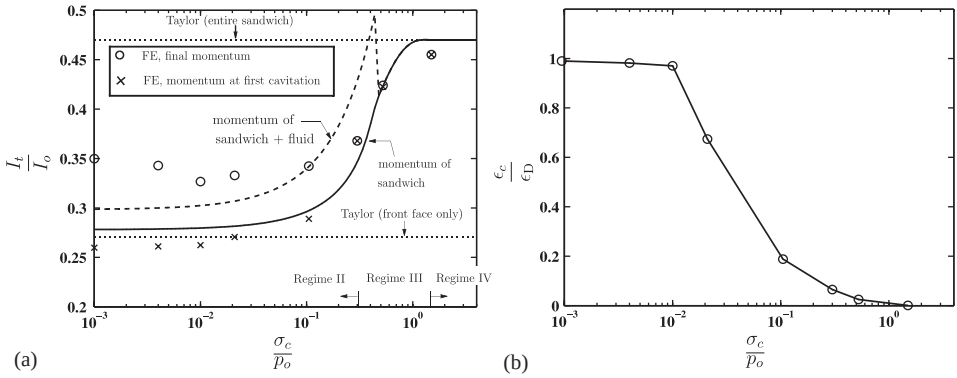

Fig. 14. (a) Comparison between the lumped parameter model and FE predictions of the momentum transmitted into the sandwich plate and (b) FE predictions of the core compression as a function of the core strength σ_c. ($\bar{I} = 0.5$, $\bar{m} = 1.0$ and $\psi = 1.75$.)

parameter model predicts that the location of the cavitation plane changes discontinuously across the regime II–III boundary which results in the discontinuity in the dashed line in Fig. 14a. Predictions by the Taylor analysis for the momentum transmitted into the sandwich plate based on (i) a free-standing front face sheet of mass m_f and (ii) a free standing monolithic plate of mass $2m_f + m_c$ are included in Fig. 14a as limits on the transmitted impulse. A comparison between the lumped parameter model and the FE calculations indicates that while the lumped parameter model accurately predicts the momentum of the sandwich plate at first cavitation[4] it is unable to capture accurately the final momentum of the sandwich plates especially for low values of $\bar{\sigma}$. The inclusion of the added fluid momentum at cavitation in the lumped parameter model improves the agreement between the two sets of calculations but is insufficient to give an accurate prediction of the final momentum of the sandwich plate. This is consistent with the fact that clean separation does not occur at the cavitation plane, as discussed in Section 3.2.3. Subsequently, predictions of the lumped parameter model are given only for the momentum of the sandwich plate at first cavitation.

Next, consider the effect of the magnitude of the shock momentum $\bar{I} \equiv I_0\theta/(m_f c\varepsilon_D)$ on the momentum transmitted into the sandwich plate for the choice $\psi = 1.75$. Finite element predictions of the final momentum of the sandwich plate are plotted as a function of $\bar{I}$ in Fig. 15 for three choices of the core strength $\bar{\sigma} = 0.01$, 0.105 and 0.525. In these FE calculations, $\bar{I}$ was varied by varying the core densification strain ε_D while keeping the shock properties fixed at their reference values. Predictions of the lumped parameter model for the momentum of the sandwich plate at first cavitation are included in Fig. 15. Consider first the choice

[4]The FE predictions of the momentum at first cavitation are slightly below the lumped parameter model predictions due to elastic effects in the sandwich plate: the lumped parameter model assumes rigid faces and a rigid–plastic core, while the FE calculations assume a finite elastic modulus in the face sheets and the core.

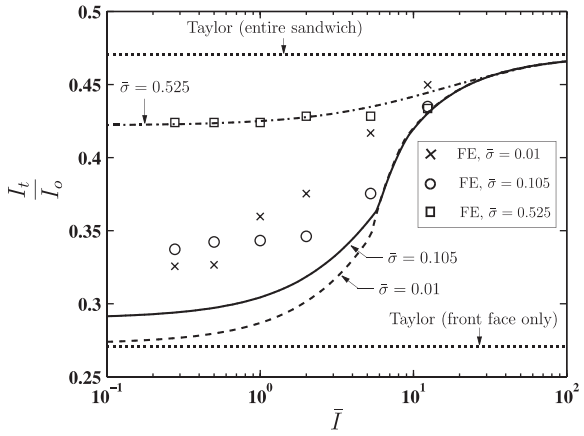

Fig. 15. Comparison between the lumped parameter and FE calculations of the momentum transmitted into the sandwich plate as a function of the shock impulse for selected values of the core strength $\bar{\sigma}$. The various regimes of behaviour in relation to the fluid–structure interaction map are discussed in the text. ($\bar{m} = 1.0$ and $\psi = 1.75$.)

$\bar{\sigma} = 0.525$. Over the full range of $\bar{I}$ shown, the response is in regime III, and the sandwich plate resembles a monolithic plate of mass $2m_f + m_c$; in this regime the lumped parameter model is adequate. Second, consider the cases $\bar{\sigma} = 0.01$ and 0.105. At high $\bar{I} \geqslant 5$, full densification of the core occurs before cavitation and the response lies in regime I. Again, the lumped parameter model closely mimics the FE calculations. At lower values of $\bar{I} < 5$, the response is in regime II, and continued loading of the sandwich plate occurs after first cavitation. Consequently, the lumped parameter model is unable to capture the response post-cavitation and thereby under-predicts the momentum imparted; this behaviour is in line with that discussed in connection with Fig. 14a.

The effect of the core mass upon the level of transmitted momentum is investigated in Fig. 16. Here, the transmitted momentum is plotted as a function of the shock impulse $\bar{I}$, for a fixed core strength $\bar{\sigma} = 0.105$ and $\psi = 1.75$. FE and lumped parameter calculations are shown for the choices of $\bar{m} = 1.0$ and 0.1. In the FE calculations $\bar{m}$ was reduced from 1.0 to 0.1 by reducing the density of the core material from the reference value of $800 - 80\,\mathrm{kg\,m^{-3}}$, and $\bar{I}$ was varied by changing the core densification strain. The results of both the FE and lumped parameter models indicate that a reduction in $\bar{m}$ leads to a smaller fraction of the shock impulse being transmitted into the sandwich plate. The reduction is most dramatic at high values of $\bar{I}$, where the sandwich plates behave like monolithic plates: a lower value of $\bar{m}$ results in a lighter sandwich plate, and hence it absorbs a smaller fraction of the shock impulse, as would be expected from the Taylor analysis.

Finally, we consider the effect of the magnitude of ψ on the momentum transmitted into the sandwich plates, for a core mass $\bar{m} = 1.0$ and for a shock impulse $\bar{I} = 0.5$. The predictions of the finite element and lumped parameter models for the final momentum of the sandwich plates are plotted in Fig. 17 as a function of

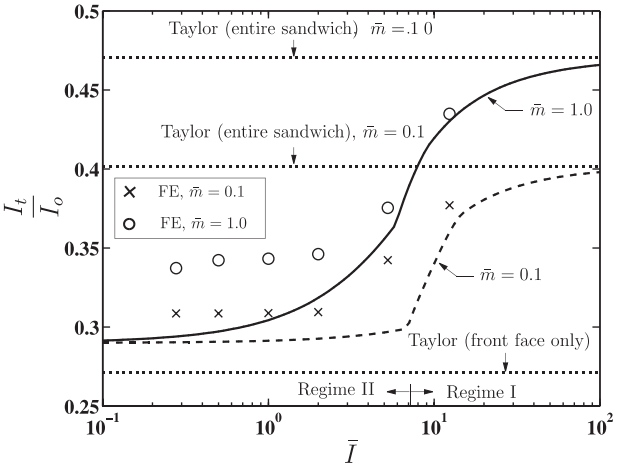

Fig. 16. Comparison between the lumped parameter and FE calculations of the momentum transmitted into the sandwich plate as a function of the shock impulse for selected values of core mass ratio $\bar{m}$ with all other properties kept at the reference values. ($\bar{\sigma} = 0.105$ and $\psi = 1.75$.)

ψ, for two choices of the core strength $\bar{\sigma}$. All other properties of the sandwich plate and the applied shock are held fixed at their reference values. In the FE calculations ψ was varied by changing the density and bulk modulus of the fluid while keeping the wave speed fixed at the reference values of $c_w = 1400\,\mathrm{m\,s^{-1}}$. The predictions of the lumped parameter model for the momentum transmitted into the sandwich plate at first cavitation are included in Fig. 17, along with the Taylor predictions for a free-standing front face of the sandwich plate and for a monolithic plate of mass equal to that of the sandwich plate. Again, the lumped parameter model is in good agreement with the FE predictions for $\bar{\sigma} = 0.525$; however, the lumped parameter model under-predicts the transmitted momentum for the case of a weak core, $\bar{\sigma} = 0.105$, when ψ exceeds unity. In all cases, the two Taylor predictions bound the more sophisticated predictions of the lumped parameter model and the finite element model.

The fluid–structure interaction map ($\bar{I} = 0.5$ and $\bar{m} = 1.0$) of Fig. 12 is re-plotted in Fig. 18 with $10^{-2} \leqslant \bar{\sigma} \leqslant 2.0$ and $0.4 \leqslant \psi \leqslant 4.0$. Contours of the transmitted impulse at first cavitation by the lumped parameter model, and the final momentum of the sandwich plates as predicted by the FE calculations are included in Fig. 18. In the FE calculations, ψ was varied by keeping (p, θ) fixed at their reference values and varying the fluid properties (E_w, ρ_w) while keeping the wave speed in the fluid fixed at $c_w = 1400\,\mathrm{m\,s^{-1}}$. For any given value of ψ, the lumped parameter model under-predicts the transmitted shock momentum in regime II but agrees well with the FE calculations in regimes III and IV. As discussed above, this discrepancy is mainly due to the fact that the lumped parameter model does not attempt to analyse the fluid–structure interaction after first cavitation.

In summary, the lumped parameter model accurately models the fluid–structure interaction problem up to first cavitation. However, the finite element simulations suggest that approximately 20% additional momentum is transmitted into the

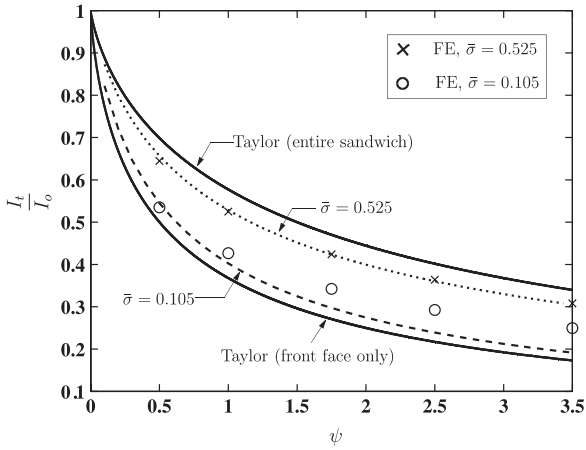

Fig. 17. Comparison between the lumped parameter and FE calculations of the momentum transmitted into the sandwich plate as a function of Taylor fluid–structure interaction parameter ψ for selected values of the core strength $\bar{\sigma}$ with all other properties kept fixed at the reference values. The $\bar{\sigma} = 0.105$ and 0.525 cases lie in regimes II and III, respectively of the fluid–structure interaction map. ($\bar{I} = 0.5$ and $\bar{m} = 1.0$.)

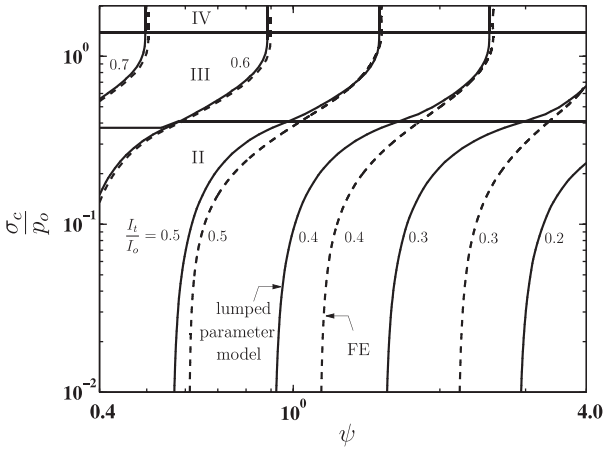

Fig. 18. Comparison between FE and lumped parameter model predictions for the fluid–structure interaction map ($\bar{I} = 0.5$, $\bar{m} = 1.0$) with axes of core strength σ_c/p_0 and the Taylor fluid–structure interaction parameter ψ. Contours of the impulse transmitted into the sandwich plate at first cavitation using the lumped parameter model and final transmitted impulse as predicted by the FE calculations are included in the map.

structure after first cavitation. This post cavitation behaviour is not modelled by the lumped parameter model. The calculations presented here suggest that adding the momentum of the fluid trapped between the structure and the cavitation plane to the impulse transmitted at first cavitation improves the agreement between the FE and lumped parameter models.

4. Implications for sandwich core design

In the above analysis, core strength and core density are treated as independent variables. Now we consider two representative core topologies and assume a particular relation between the strength and density of each core.

Metallic cellular sandwich cores may be classified into stretching-governed and bending-governed topologies. Stretching-governed cores deform by the plastic stretching of the constituent struts and consequently have a strength σ_c which scales linearly with the relative density $\bar{\rho}$. Examples include the Octet truss and pyramidal core, see Wadley et al. (2004) for a detailed discussion. Bending-governed cores deform by the plastic bending of the constituent struts and consequently have a strength σ_c which scales as $\bar{\rho}^{3/2}$. Examples include metal foams, see Ashby et al. (2000) for further details. Here, we analyse the response of sandwich plates with these two prototypical cores. It is assumed that the stretching and bending governed cores have a strength versus relative density relationships given by

$$\frac{\sigma_c}{\sigma_Y} = 0.5\bar{\rho}, \tag{48a}$$

and

$$\frac{\sigma_c}{\sigma_Y} = 0.3\bar{\rho}^{3/2}, \tag{48b}$$

respectively. These expressions are representative of the Octet truss (Deshpande et al., 2001) and metal foams (Ashby et al., 2000), respectively. The densification strain is assumed to be related to $\bar{\rho}$ via (Ashby et al., 2000)

$$\varepsilon_D = 0.8 - 1.75\bar{\rho}. \tag{48c}$$

Finite element calculations were performed on sandwich plates comprising face sheets of thickness $h = 10$ mm, made from the reference face sheet material ($\rho_f = 8000\,\mathrm{kg\,m^{-3}}$, and $E_f = 210\,\mathrm{GPa}$) with a core to face sheet mass ratio $\bar{m} = 1.0$. The core was assumed to be made from the same solid material as the face sheets, with a solid yield strength σ_Y taken to be 210 MPa, which is representative of most structural steels, and a core density $\rho_c = \bar{\rho}\rho_f$. The core was taken to have a strength and nominal densification strain as specified by (48), and a Young's $E_c = 1000\sigma_c$. For a given mass of core $\bar{m}$, the core thickness varies inversely with $\bar{\rho}$ and is given by

$$c = \frac{\bar{m}}{\bar{\rho}}\, h. \tag{49}$$

In all the FE calculations, the fluid medium was assumed to be water with $\rho_w = 1000\,\mathrm{kg\,m^{-3}}$ and $c_w = 1400\,\mathrm{m\,s^{-1}}$, and the sandwich plate was subjected to the reference shock $p_0 = 100\,\mathrm{MPa}$ and $\theta = 0.1\,\mathrm{m\,s}$. Thus, the non-dimensional groups held constant in these calculations are $\bar{m} = 1.0$, $\psi = 1.75$, $\sigma_Y\theta/I_0 = 1.05$ and $I_0\theta/(m_f h) = 2.5$.

The FE predictions of the final momentum transmitted into the sandwich plate are plotted in Fig. 19 for both the *bending* and *stretching* governed cores. The predictions of the lumped parameter model for the transmitted momentum at first cavitation,

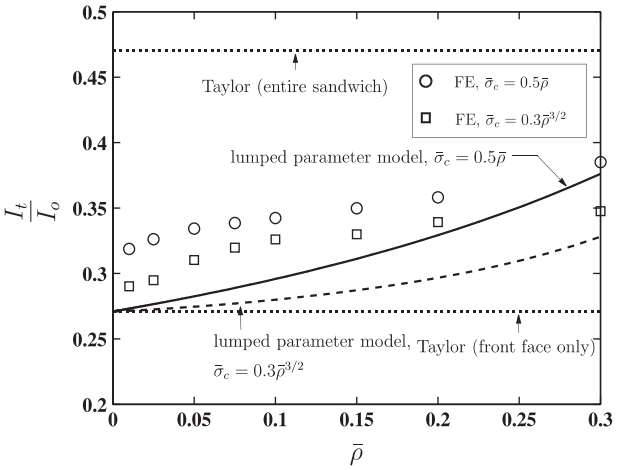

Fig. 19. Comparison between the lumped parameter and FE calculations of the momentum transmitted into the sandwich plate as a function of the relative density $\bar{\rho}$ of the core for two types of cores. In these calculations, $\bar{\rho}$ was varied with $\bar{m} = 1.0$, $\psi = 1.75$, $\sigma_Y\theta/I_0 = 1.05$ and $I_0\theta/(m_f h) = 2.5$ kept constant.

and the Taylor predictions based on the front face only and the entire sandwich plate are included. The following main points can be drawn from Fig. 19:

(a) The momentum transmitted into the sandwich plates is substantially lower than that into a monolithic plate of same mass.
(b) The Taylor analysis, based upon the front face only, and the lumped parameter model underestimate the momentum transmitted into the sandwich plate.
(c) For a given core relative density, a smaller fraction of the shock impulse is transmitted into the sandwich plates with the bending-governed cores. This is a result of the lower compressive strength of the bending governed cores.

In addition to the transmitted impulse, the FE results for the final average through thickness core compressive strain ε_c and the total loading time T_{fs} are plotted in Figs. 20a and b, respectively. While complete densification does not occur for any of the cases analysed here, ε_c for the bending-governed cores increases from ≈ 0.2 to 0.6 as $\bar{\rho}$ decreases from 0.3 to 0.01. On the other hand, ε_c is almost constant at about 0.1 for the stretching governed cores over the range $0.01 \leqslant \bar{\rho} \leqslant 0.3$. The core compression times T_{fs} also increase with decreasing $\bar{\rho}$, with T_{fs} being much longer for the bending governed cores than for the stretching governed cores. In fact, $T_{\text{fs}} \approx 30$ ms for the bending governed core of $\bar{\rho} = 0.01$. In such cases the separation of time scales between the core compression phase and the beam bending and stretching phases, as assumed by Fleck and Deshpande (2004), does not occur. Consequently, the Fleck and Deshpande (2004) analysis for a clamped beam would over-predict the deflection.

In summary, bending governed sandwich cores result in a smaller fraction of the shock impulse being transmitted into the structure and in longer core compression

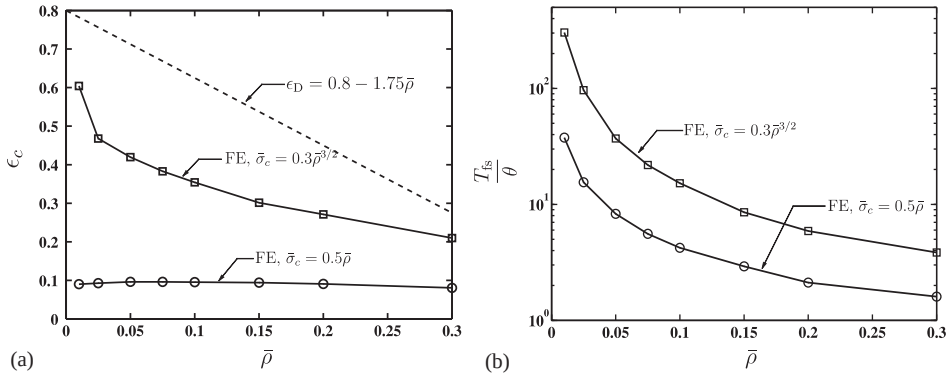

Fig. 20. FE predictions of (a) the core compression strain and (b) duration of the fluid–structure interaction phase as a function of the core relative density $\bar{\rho}$ of the core for two types of cores. In these calculations, $\bar{\rho}$ was varied with $\bar{m} = 1.0$, $\psi = 1.75$, $\sigma_Y\theta/I_0 = 1.05$ and $I_0\theta/(m_f h) = 2.5$ kept constant.

times than stretching governed cores. This would result in an enhanced shock resistance of the sandwich beams (or plates). On the other hand, the higher degree of core compression results in a loss in the bending strength of the sandwich beams (or plates) and this will reduce the structural resistance to shock loading. A full analysis of the beam or plate including the consideration of the bending and stretching response is required in order to determine the optimal core design.

5. Concluding remarks

In this paper, the one-dimensional shock response of sandwich plates subject to both impulsive loading and to an underwater pressure pulse has been investigated. Both the propagation of an impinging acoustic shock wave within the fluid, and the propagation of a plastic shock wave within the sandwich core are accounted for. The degree of strain hardening in the core has a negligible effect on the core compression for realistic ratios of core to face sheet mass: the energy dissipation associated with the plastic shock wave is much greater than that in quasi-static dissipation.

The FE fluid–structure interaction calculations and the lumped parameter model reveal that cavitation does not necessarily occur at the fluid–structure interface of a sandwich plate. Moreover, the FE calculations show that clean crack-like separation does not occur at the first cavitation plane; rather, a cavitated zone of bubbly fluid broadens from the first cavitation plane. Momentum is transferred into the sandwich up to the end of the core compression phase. While the lumped parameter model accurately predicts the momentum of the sandwich plate at first cavitation, the model is not sufficiently sophisticated to capture subsequent wave propagation effects within the cavitated fluid. Thus, the lumped parameter model captures the final momentum of the sandwich plate to limited accuracy. Both the lumped parameter model and the FE calculations show that the fraction of the shock

momentum transmitted into the sandwich plate increase with increasing core strength, total shock impulse and mass of sandwich plate.

Fleck and Deshpande (2004) and Xue and Hutchinson (2004) estimated the momentum transmitted into a sandwich plate using the Taylor analysis for a free standing front face sheet. The accuracy of this assumption depends upon the magnitude of the core strength (Fig. 14), the imposed impulse (Fig. 15), the mass ratio of the core to face sheet, $m\bar{m}$, (Fig. 16) and more mildly upon the value of the fluid–structure interaction parameter ψ. The choice $\bar{I} = 0.5$, $m\bar{m} = 1.0$ and $\psi = 1.75$ is taken to be representative of that for an underwater shock on a steel structure. In this case, the FE analysis presented here demonstrates that the Taylor model underestimates the transmitted impulse by about 20% for $\bar{\sigma} < 0.1$; see Fig. 14a. Further, the analysis suggests that sandwich cores with a low strength such as the Y-core developed by Schelde Shipbuilding[5] might be beneficial from a fluid–structure interaction perspective: optimisation of the sandwich core properties to minimise the transmitted impulse and maximise sandwich strength remains a topic for future investigation.

Acknowledgements

The authors are grateful to ONR for their financial support through US-ONR IFO Grant number N00014-03-1-0283 on the The Science and Design of Blast Resistant Sandwich Structures. We are pleased to acknowledge Profs. T. Belytschko, A.G. Evans and J.W. Hutchinson for many insightful discussions during the course of this work.

Appendix A. Prescription for the artificial core viscosity in the FE calculations and FE predictions for the impulse loading of sandwich plates

The prescription for choosing the viscosity η in the rate dependent constitutive law (34) and the associated choice of the finite element mesh size e employed in the core are discussed in this Appendix.

Dynamic compression of a rate dependent foam gives rise to a shock of finite width as discussed in Radford et al. (2005). For a linear viscous foam, the shock width l is given by (Radford et al., 2005)

$$l = \frac{\eta \varepsilon_D}{\rho \Delta v}, \tag{A.1}$$

where η is the linear viscosity, ρ the initial foam density and Δv the velocity jump across the shock. In the finite element calculations, we choose η such that the shock width l is much less than the core thickness c to ensure that the artificial viscosity η does not significantly affect the structural response.

[5]Royal Schelde, P.O. Box 16 4380 AA Vlissingen, The Netherlands.

To determine the shock width l, we need to estimate the velocity jump Δv. Here, we employ the estimate $\Delta v = p_0\theta/m_f$ based upon a free-standing front face sheet. Thus, in the FE calculations presented here, Δv is taken to be $125\,\mathrm{m\,s^{-1}}$ ($p_0 = 100\,\mathrm{MPa}$, $\theta = 0.1\,\mathrm{m\,s}$ and $m_f = 80\,\mathrm{kg\,m^{-2}}$) and η is chosen such that $l = 5\,\mathrm{mm}$ ($\ll c = 100\,\mathrm{mm}$). For example, for the reference core material properties ($\rho = 800\,\mathrm{kg\,m^{-3}}$, $\varepsilon_D = 0.5$), η is taken to be 1.0 kPas.

Large gradients in stress and strain occur over the shock width l. To ensure that the finite element calculations resolve these large gradients accurately, the element size e in the core was taken to satisfy the condition $e \leqslant l/20$.

We proceed to demonstrate the accuracy of the shock wave propagation model developed in Section 2.1.2 for the impulse response of the foam core sandwich plates by comparing the analytical predictions with FE calculations. Consider a free standing sandwich plate with the reference material properties described in Section 3.2.1 and a core yield strength $\sigma_c = 2$ MPa. Loading corresponding to the non-dimensional impulse $\hat{I}$ is specified by imparting an initial velocity v_0

$$v_0 = \hat{I}\sqrt{\frac{c\sigma_c\varepsilon_D}{m_f}}, \tag{A.2}$$

to the outer face-sheet of the sandwich plate. The final through-thickness nominal strain in the core ε_c is when both the sandwich face-sheets have attained a final common velocity. A comparison between the FE and analytical predictions (shock wave propagation model) of the variation of ε_c with $\hat{I}$ is shown in Fig. A.1 for the reference case of core to face sheet mass ratio $\bar{m} = 1.0$. An additional case in which $\bar{m}$ was reduced to 0.1 was also analysed by reducing the core thickness to $c = 10$ mm with all other properties kept fixed at their reference values. The FE and analytical calculations are in excellent agreement for both $\bar{m} = 1.0$ and 0.1. Moreover, increasing the core modulus E_c from the reference value of 10^3–$10^4\sigma_c$ had a negligible effect on the core compression. This confirms the accuracy and validity of the rigid–plastic analytical model presented in Section 2.1.2 and also shows that the rigid–plastic analysis is adequate for practical values of the core Young's modulus. Note that in all these FE calculations the viscosity η was chosen such that shock width l equals $c/20$ with Δv in (A.1) set equal to v_0.

Appendix B. A simplified fluid–structure interaction model for sandwich plates

The Taylor analysis of the fluid–structure interaction for a shock-loaded free-standing plate can be extended to the case of a rigid plate on a plastic foundation in order to make an approximate estimate for the fluid–structure interaction of sandwich plates. We assume that the front face of the sandwich plate is accelerated by the shock impulse while its motion is resisted by a core of strength σ_c. Simultaneously, the rear face is accelerated by the pressure σ_c from the core. The mass of the core is neglected and so shock wave effects are neglected. Here, we develop this simplified analysis and contrast it with the lumped parameter shock

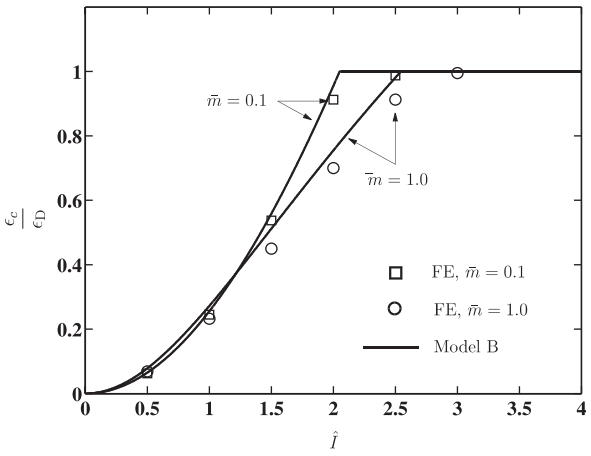

Fig. A.1. Finite element predictions of the core compression as a function of the normalised shock impulse for two choices of the core to face sheet mass ratio $\bar{m}$. The analytical plastic shock wave propagation model (Model B) predictions are also included.

wave model and the FE calculations reported above. Further details of such an analysis are given in Hutchinson and Xue (2005).

Consider a plate of mass m_f on a plastic foundation of strength σ_c. An incoming wave in the fluid of density ρ_w, travels with a constant velocity c_w in the direction of increasing x measured along the inward normal to the plate. Upon making the usual assumption that the pressure profile for blast wave can be taken to be of the exponential form (22), the equation of motion of the plate is given by

$$2p_0 e^{-t/\theta} - \rho_w c_w v - \sigma_c = m_f \dot{v}, \tag{B.1}$$

where v is the velocity of the plate. This ODE, with initial conditions $v = 0$ at time $t = 0$, admits the solution

$$v = \frac{2p_0\theta}{m_f(\psi - 1)}\left[e^{-t/\theta} - e^{-t\psi/\theta}\right] + \frac{\sigma_c}{\rho_w c_w}\left[e^{-t\psi/\theta} - 1\right]. \tag{B.2}$$

Thus, the pressure $\bar{p} \equiv p/p_0$ at a distance x from the plate (x is measured as negative into the fluid) is given by

$$\bar{p} = -\frac{2}{\psi - 1}\left[\cosh\,\bar{x} - \psi \sinh\,\bar{x}\right]e^{-\bar{t}} + \left(\frac{2\psi}{\psi - 1} - \bar{\sigma}\right)e^{-\psi\bar{t} - \psi\bar{x}} + \bar{\sigma}, \tag{B.3}$$

where $\bar{t} \equiv t/\theta$, $\bar{x} = x/(c_w\theta)$ and $\psi \equiv \rho_w c_w \theta/m_f$. First cavitation occurs when $\bar{p} = 0$ and $\partial p/\partial \bar{x} = 0$. Employing these conditions, the distance x_c of the cavitation plane from the plate is given by

$$\ln\left[\frac{2(1+\psi)\sinh\bar{x}_c}{\bar{\sigma}\psi}\right] = \frac{1}{1-\psi}\left[\ln\left(\frac{\psi\cosh\bar{x}_c + \sinh\bar{x}_c}{\psi^2 - 0.5\bar{\sigma}\psi(\psi-1)}\right) - \psi\bar{x}_c\right], \tag{B.4}$$

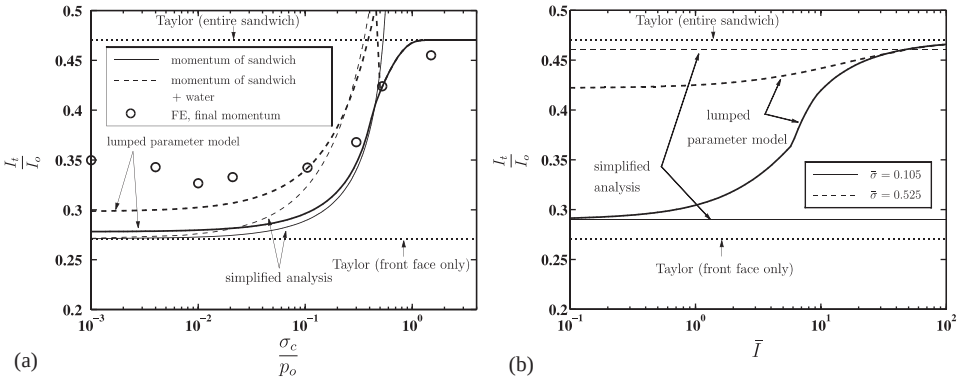

Fig. B.1. Comparison between the full lumped parameter, simplified analytical and FE predictions of the transmitted impulse for a sandwich plate with $\bar{m} = 1.0$ and $\psi = 1.75$. (a) Transmitted impulse as a function of the core strength $\bar{\sigma}$ with $\bar{I} = 0.5$ and (b) transmitted impulse as a function of the shock impulse $\bar{I}$ for two selected values of the core strength $\bar{\sigma}$; the impulse neglects the momentum of the water between the cavitation plane and the front face of the sandwich plate.

where $\bar{x}_c = x_c/(c_w\theta)$ and the corresponding cavitation time $\bar{t}_c \equiv t_c/\theta$ is

$$\bar{t}_c = \ln\left[\frac{2(1+\psi)\sinh \bar{x}_c}{\bar{\sigma}\psi}\right]. \tag{B.5}$$

Thus, the momentum of the sandwich plate (front and rear face) at the instant of cavitation is given by

$$\frac{I_t}{I_0} = \frac{1}{\psi - 1}\left[e^{-\bar{t}_c} - e^{-\psi\bar{t}_c}\right] + \frac{\bar{\sigma}}{2\psi}\left[e^{-\psi\bar{t}_c} - 1\right] + \frac{\bar{\sigma}\bar{t}_c}{2}. \tag{B.6}$$

The momentum of the fluid trapped between the front face of the sandwich plate and the cavitation plane follows from (45) as

$$\frac{I_w}{I_0} = \frac{1}{2}\left[2e^{-\bar{t}_c} - e^{-\bar{t}_c-\bar{x}_c} - e^{-\bar{t}_c+\bar{x}_c}\right] + \frac{\psi}{\psi-1}\left[e^{-\bar{t}_c-\bar{x}_c} - e^{-\bar{t}_c} - \frac{1}{\psi}\left(e^{-\psi(\bar{t}_c+\bar{x}_c)} - e^{-\psi\bar{t}_c}\right)\right] + \frac{\bar{\sigma}\psi}{2}\left[e^{-\psi(\bar{t}_c+\bar{x}_c)} - e^{-\psi\bar{t}_c}\right] + \frac{\bar{\sigma}\bar{x}_c}{2}. \tag{B.7}$$

A comparison between the predictions of the momentum transmitted to the sandwich plate ($\bar{I} = 0.5$, $\bar{m} = 1.0$ and $\psi = 1.75$) employing this simplified analysis, the full lumped parameter, and FE calculations is shown in Fig. B.1a for $10^{-3} \leqslant \bar{\sigma} \leqslant 0.4$. The simplified analysis agrees well with the full analysis for $\bar{\sigma} < 0.05$ but predictions of the two analyses diverge for large $\bar{\sigma}$, with the simplified analysis not reducing to the Taylor prediction in the limit of large $\bar{\sigma}$. Neither the full lumped parameter model nor the above simplified analysis capture the FE predictions sufficiently accurately over the entire range of $\bar{\sigma}$. The simplified analysis predicts that the ratio of transmitted shock impulse to I_0 is independent of $\bar{I}$ and hence does not capture the increase in the fractional transmitted momentum with $\bar{I}$. This is

illustrated in Fig. B.1b for $\bar{m} = 1.0$, $\psi = 1.75$ and $\bar{\sigma} = 0.105$. Thus, the simplified analysis can be thought of as a first order perturbation on the Taylor analysis.

References

Ashby, M.F., Evans, A.G., Fleck, N.A., Gibson, L.J., Hutchinson, J.W., Wadley, H.N.G., 2000. Metal Foams: A Design Guide. Butterworth, Heinemann, London.

Bland, D.R., 1988. Wave Theory and Applications. Oxford University Press, Oxford.

Bleich, H.H., Sandler, I.S., 1970. Interaction between structures and bilinear fluids. Int. J. Solids Struct. 6 (5), 617–639.

Deshpande, V.S., Fleck, N.A., Ashby, M.F., 2001. Effective properties of the octet-truss lattice material. J. Mech. Phys. Solids 49 (8), 1747–1769.

Duvall, G.E., 1973. Shock waves and equations of state. In: Chou, P.C., Hopkins, A.K. (Eds.), Dynamic Response of Materials to Intense Loading. Air Force Materials Laboratory, OH, USA, pp. 89–121.

Fleck, N.A., Deshpande, V.S., 2004. The resistance of clamped sandwich beams to shock loading. J. Appl. Mech. 71 (3), 386.

Hutchinson, J.W., Xue, Z., 2005. Metal sandwich plates optimised for pressure impulses. Int. J. Mech. Sci. 47 (4–5), 545–569.

Kennard, E.H., 1943. Cavitation in an elastic liquid. Phys. Rev. 63 (5–6), 172–181.

Krieg, R.O., Key, S.W., 1973. Transient shell response by numerical time integration. Int. J. Numer. Meth. Eng. 7, 273–286.

Mäkinen, K., 1999. Underwater shock loaded sandwich structures. Ph.D. Thesis, Royal Institute of Technology, Department of Aeronautics, Stockholm, Sweden.

Rabczuk, T., Kim, J.Y., Samaniego, E., Belytschko, T., 2004. Homogenization of sandwich structures. Int. J. Numer. Meth. Eng. 61 (7), 1009–1027.

Radford, D.D., Deshpande, V.S., Fleck, N.A., 2005. The use of metal foam projectiles to simulate shock loading on a structure. Int. J. Impact Eng. 31 (9), 1152–1171.

Reid, S.R., Peng, C., 1997. Dynamic uniaxial crushing of wood. Int. J. Impact Eng. 19, 531.

Sprague, M.A., 2002. Advanced computational techniques for the analysis of 3-D fluid-structure interaction with cavitation. Ph.D. Thesis, University of Colorado, Boulder, USA.

Tan, P.J., Harrigan, J.J., Reid, S.R., 2002. Inertia effects in the uniaxial dynamic compression of a closed-cell aluminium alloy foam. Mater. Sci. Tech. 18, 480–488.

Taylor, G.I., 1941. The Scientific Papers of G I Taylor, vol. III, Cambridge University Press, Cambridge, 1963. (The pressure and impulse of submarine explosion waves on plates, pp. 287–303).

Temperley, H.N.V., 1950. Theoretical investigation of cavitation phenomena occurring when an underwater pressure pulse is incident on a yielding surface. Underwater Explosions Research, vol. III, The Damage Process, Office of Naval Research, pp. 260–268.

Wadley, H.N.G., Fleck, N.A., Evans, A.G., 2004. Fabrication and structural performance of periodic cellular metal sandwich structures. Composite Sci. Technol. 63 (16), 2331.

Xu, X.P., Needleman, A., 1994. Numerical simulations of dynamic crack-growth along an interface. J. Mech. Phys. Solids 42, 1397–1434.

Xue, Z., Hutchinson, J.W., 2004. A comparative study of blast-resistant metal sandwich plates. Int. J. Impact Eng. 30 (10), 1283–1305.